Design and Analysis of Non-Orthogonal Multiple Access Techniques for Terahertz Networks

Sadeq Bani Melhem

A THESIS SUBMITTED TO THE FACULTY OF GRADUATE STUDIES IN PARTIAL FULFILLMENT OF THE REQUIREMENTS FOR THE DEGREE OF MASTER OF APPLIED SCIENCE
GRADUATE PROGRAM IN ELECTRICAL ENGINEERING AND COMPUTER SCIENCE

YORK UNIVERSITY
TORONTO, ONTARIO

January 2022

Abstract

Fueled by the emergence of machine-type communications in a variety of wireless applications, the provisioning of massive connectivity becomes instrumental. On the other hand, accommodating trillions of devices within the extremely congested and limited sub-6GHz spectrum is becoming challenging. In this context, shifting to higher frequency terahertz (THz) communication is under consideration to obtain the data rates in the order of hundreds of gigabits per second (Gbps). Also, non-orthogonal multiple access schemes are becoming popular to support multiple users in the same frequency and time resource block, while leveraging on efficient interference cancellation mechanisms.

In this thesis, I develop a comprehensive mathematical framework to analyze the performance of emerging non-orthogonal channel access schemes, such as non-orthogonal multiple access (NOMA) and rate-splitting multiple access (RSMA), in THz networks. In the first part of the thesis, I develop a statistical framework to analyze the performance of NOMA in the downlink of a single-carrier and multi-carrier THz network considering Nakagami-m fading and molecular absorption noise. In this context, I first develop a novel user pairing scheme which ensures the performance gains of NOMA over orthogonal multiple access (OMA) for each individual user in the NOMA pair and adapts according to the THz molecular absorption. Then,

I characterize novel outage probability expressions considering a single-carrier and multi-carrier THz-NOMA network in the presence of various user pairing schemes, Nakagami-m channel fading, and molecular absorption noise. Specifically, I propose a moment-generating-function (MGF) based approach to analyze the outage probability of users in a multi-carrier THz network. For negligible thermal noise, I provide simplified single-integral expression to compute the outage in a multi-carrier network. Numerical results demonstrate the efficiency of the proposed user-pairing scheme compared to the existing benchmarks and validate the accuracy of the derived expressions. Finally, in the second part of the thesis, I extend the developed framework to analyze the performance of RSMA in the downlink transmission of Sub-6 GHz and THz networks.

Acknowledgments

First and foremost I would like to thank Allah Almighty for His immense blessings and help throughout the duration of MASc program. I would like also to express my earnest gratefulness to my advisor Professor Hina Tabassum for the enormous support during my study and enhancing my knowledge in the field of wireless communications. Her reviews, insightful comments, encouragement, and legitimate guidelines aided me to develop the contents of my research work. Furthermore, I would like to thank my thesis committee members, Professor Uyen Trang Nguyen and Professor Mehdi Nourinejad, they gave their valuable feedback and nominate this thesis for the best thesis award at Lassonde School of Engineering with utmost satisfaction for outstanding dissertation. I convey special acknowledge to Professor Mufleh Al-Shatnawi for his support and recommendation.

Finally, I want to thank my beloved sisters, brothers and parents, Younis Bani Melhem and Manahel Bani Melhem, for their continuous encouragement and love. I want to thank my wife for her patience and bearing with me for my negligence towards her during this journey, and my daughters Ghalia and Asal for their infinite affection and love. I hope that Allah will provide me with the opportunity to return them the kindness, the support and the patience they have always shown me.

Contents

Abstract ii

Acknowledgments iv

Contents v

List of Figures viii

Abbreviations x

Research Outcomes xiv

1 Introduction 1
- 1.1 Evolution of Transmission Spectrum . . . 2
  - 1.1.1 Sub-6GHz Spectrum . . . 3
  - 1.1.2 mm-Wave Spectrum . . . 3
  - 1.1.3 THz Spectrum . . . 4
- 1.2 Evolution of Multiple Access Schemes . . . 4
  - 1.2.1 Orthogonal Multiple Access (OMA) . . . 5
  - 1.2.2 Non-Orthogonal Multiple Access (NOMA) . . . 8
  - 1.2.3 Rate Splitting Multiple Access (RSMA) . . . 10
- 1.3 Challenges . . . 12
  - 1.3.1 Molecular Absorption and Propagation Modeling . . . 12
  - 1.3.2 Multi-Carrier Transmissions . . . 13
  - 1.3.3 User Pairing in THz Network . . . 13
- 1.4 Contributions . . . 14
- 1.5 Thesis Outline . . . 15

2 Mathematical Preliminaries and Literature Review 17
- 2.1 Key Performance Indicators . . . 17
  - 2.1.1 Signal to Interference Plus Noise Ratio (SINR) . . . 17
  - 2.1.2 Data Rate . . . 18

2.1.3 Outage Probability (OP) . . . 18
2.2 Mathematical Preliminaries . . . 19
2.2.1 Order Statistics . . . 19
2.2.2 Moment-Generating Function (MGF) . . . 20
2.2.3 Gil-Pelaez Inversion Theorem . . . 21
2.3 Literature Review . . . 22
2.3.1 THz-NOMA . . . 23
2.3.2 RSMA . . . 24
2.4 Summary . . . 26

3 Outage Analysis in Multi-Carrier NOMA-THz Networks 27
3.1 Motivation/Contribution . . . 27
3.2 System model and Assumptions . . . 28
3.2.1 Molecular Absorption Coefficient . . . 30
3.2.2 THz LoS Channel Model . . . 32
3.2.3 Fading Model . . . 32
3.2.4 Antenna Model . . . 33
3.2.5 SINR - NOMA Model . . . 34
3.2.6 SINR - OMA Model . . . 35
3.3 Outage Analysis: Single-Carrier THz-NOMA . . . 36
3.3.1 Proposed User Grouping Scheme . . . 37
3.3.2 OP Analysis . . . 39
3.4 Outage Analysis: Multi-Carrier THz-NOMA . . . 41
3.5 Numerical Results and Discussions . . . 44
3.6 Summary . . . 48

4 Outage Analysis in RSMA Networks 50
4.1 Motivation/Contribution . . . 50
4.2 System Model and Assumptions . . . 51
4.2.1 Channel Model . . . 53
4.2.2 SINR Model: Common message . . . 54
4.2.3 SINR Model: Private Messages . . . 55
4.2.4 Data Rate . . . 55
4.3 General Outage Analysis: RSMA . . . 56
4.4 Outage Analysis: RSMA-RF Network . . . 58
4.4.1 Near User . . . 58
4.4.2 Far User . . . 60
4.5 Outage Analysis: RSMA-THz Network . . . 61
4.5.1 Near User . . . 61
4.5.2 Far User . . . 63

4.6 Numerical Results and Discussions 65
4.7 Summary 67

5 Conclusions and Future Directions **69**
5.1 Conclusion 69
5.2 Future Directions 70
5.2.1 Reducing NOMA Implementation Complexity 70
5.2.2 Transmitter Design 70
5.2.3 Imperfect CSI 71
5.2.4 Non-line-of-sight (NLOS) propagation for THz networks . . . 71
5.2.5 Multi-bands for 6G networks 72
5.2.6 Multi-Carrier RSMA-THz Network Performance: 72
5.2.7 Novel User Pairing for THz-RSMA Network 72
5.2.8 RSMA-THz Performance for Uplink Transmissions 73
5.2.9 Optimize User Clustering 73
5.2.10 NOMA Security 73
5.2.11 Applying Machine Learning Technique: 73
5.2.12 THz Security 74

Bibliography **75**

Appendices **86**
I Appendix A 86
I.1 Proof of Lemma 1 86
I.2 Proof of Lemma 2 86
I.3 Proof of Lemma 3 87
II Appendix B 88
II.1 Proof of Corollary 1 88
II.2 Proof of Corollary 2 88

List of Figures

1.1 Electromagnetic Spectrum (`https://areeweb.polito.it/ricerca/superconductivity/PR/MONADE/index_monade.htm`). 2

1.2 Evolution of multiple access schemes over the past decades. 5

1.3 Downlink NOMA in a single cell with one AP and n users. 8

1.4 Downlink RSMA in a single cell with one AP and n users. 11

3.1 Downlink NOMA in a single cell with one AP and 2 users. 29

3.2 Downlink NOMA transmission model 29

3.3 User grouping scheme based on R_{thr_1} and R_{thr_2}. 37

3.4 Outage performance of near and far users as a function of the molecular absorption coefficient in THz spectrum considering a single-carrier network, $R = 60$ m, $\tau_1 = 3$ bps/Hz, and $\tau_2 = 0.5$ bps/Hz. 46

3.5 Outage performance of near and far users as a function of the power allocation coefficient of near user considering a single-carrier network, $k(f) = 0.03$ $R = 60$ m, $\tau_1 = 3$ bps/Hz and $\tau_2 = 0.5$ bps/Hz. 47

3.6 Outage performance of near and far users as a function of the number of subcarriers in THz spectrum, τ_1=8 bps/Hz and τ_2=0.5 bps/Hz. . 48

4.1 Downlink RSMA in a single cell with one AP and 2 users. 52

4.2 Downlink RSMA transmission model. 53

4.3 OP of near and far users as a function of the cell-radius, in RF spectrum where the power factors are given as p_1=0.20, p_2=0.25, and p_c=0.55. 66

4.4 OP of near and far users as a function of the cell-radius in THz spectrum, where the power factors are $p_1 = 0.15, p_2 = 0.30, p_c = 0.55$. . . . 67

4.5 OP of near and far users as a function of power allocation spectrum in THz spectrum, for all multiple access schemes (OMA, NOMA, and RSMA), where radius $R = 60$, $p_2 = 0.25$, $ka = 0.03\, m^{-1}$ ($f_t = 0.8$ THz). 68

Abbreviations

1G First Generation. 6

2G Second Generation. 6

3G Third Generation. 7

3GPP Third Generation Partnership Project. 7

4G Fourth Generation. 2

5G Fifth Generation. 2

6G Sixth Generation. 2

AMPS Advance Mobile Phone Service. 6

AP Access-Point. 8

BS Base-Station. 9

CDF Cumulative Density Function. 20

CDMA Code Division Multiple Access. 6

C-RAN Cloud Radio Access Network. 24

CSI Channel state information. 12

ETACS European Total Access Communication System. 6

FDMA Frequency Division Multiple Access. 6

Gbps Gigabits Per Second. ii

GHz Gigahertz. 2

GSM Global System for Mobile. 6

HITRAN HIgh Resolution TRANsmission. 30

IID Independent and Identically Distributed. 19

IS-136 Interim Standard-136. 6

IS-54 Interim Standard-54. 6

LoS Line-Of-Sight. 14

MAC Medium Access Control Layer. 1

MGF Moment-Generating-Function. iii

MISO Multi-Input Single-Output. 11

mm-Waves Millimeter-Waves. 1

MUST Multiuser Superposition Transmission. 28

NOMA Non-Orthogonal Multiple Access. ii

OFDM Orthogonal Frequency-Division Multiplexing. 7

OFDMA Orthogonal Frequency Division Multiple Access. 7

OMA Orthogonal Multiple Access. ii

OP Outage Probability. 14

PDC Personal Digital Cellular. 6

PDF Probability Density Function. 19

PHY Physical Layer. 1

QoS Quality of Service. 10

RF Radio Frequency. 1

RIS Reconfigurable Intelligent Surface. 25

RSMA Rate-Splitting Multiple Access. ii

SCA Successive Convex Approximation. 24

SC-FDMA Single Carrier Frequency-Division Multiple Access. 7

SDMA Spatial Division Multiple Accesss. 11

SIC Successive Interference Cancellation. 8

SINR Interference Plus Noise Ratio. 17

SISO Single-Input-Single-Output. 24

Tbps Terabits per second. 4

TDMA Time Division Multiple Access. 6

THz Terahertz. ii

UAV Unmanned Aerial Vehicles. 11

Research Outcomes

• Sadeq B. Melhem; Hina Tabassum, "User Pairing and Outage Analysis in Multi-Carrier NOMA-THz Networks", *IEEE Transactions on Vehicular Technology*, Impact factor (6.239), which is accepted.

• Sadeq B. Melhem; Arjun Kaushik; Hina Tabassum; Uyen T. Nguyen, "Machine Learning for Resource Allocation in Mobile Broadband Networks," Book Chapter in *Communication Networks and Service Management in the Era of Artificial Intelligence and Machine Learning*, *Wiley-IEEE Press* [1].

• Sadeq B. Melhem; Hina Tabassum, "On the Performance of RSMA in the Downlink Terahertz (THz) Network," to be submitted.

Chapter 1

Introduction

The rapid proliferation of smart wireless applications and massive connectivity requirements has made it increasingly difficult to squeeze data into the finite number of licensed radio frequency (RF) bands. In this context, various solutions are currently under investigation both at the network physical (PHY) layer and medium access control (MAC) layer to prevent wireless spectrum saturation. For instance, at the PHY layer, shifting to higher frequency millimeter-Waves (mm-Waves) [2] and terahertz (THz) [3] communication is under consideration to obtain data rates in the order of hundreds of gigabits per second (Gbps). Similarly, at the MAC layer, novel non-orthogonal channel access mechanisms such as non-orthogonal multiple access (NOMA) [4], delta of orthogonal multiple access (OMA) [5], partial NOMA, and rate splitting multiple access (RSMA) are under investigation to support multiple users in the same frequency and time resources while leveraging on efficient interference cancellation mechanisms at the receiver.

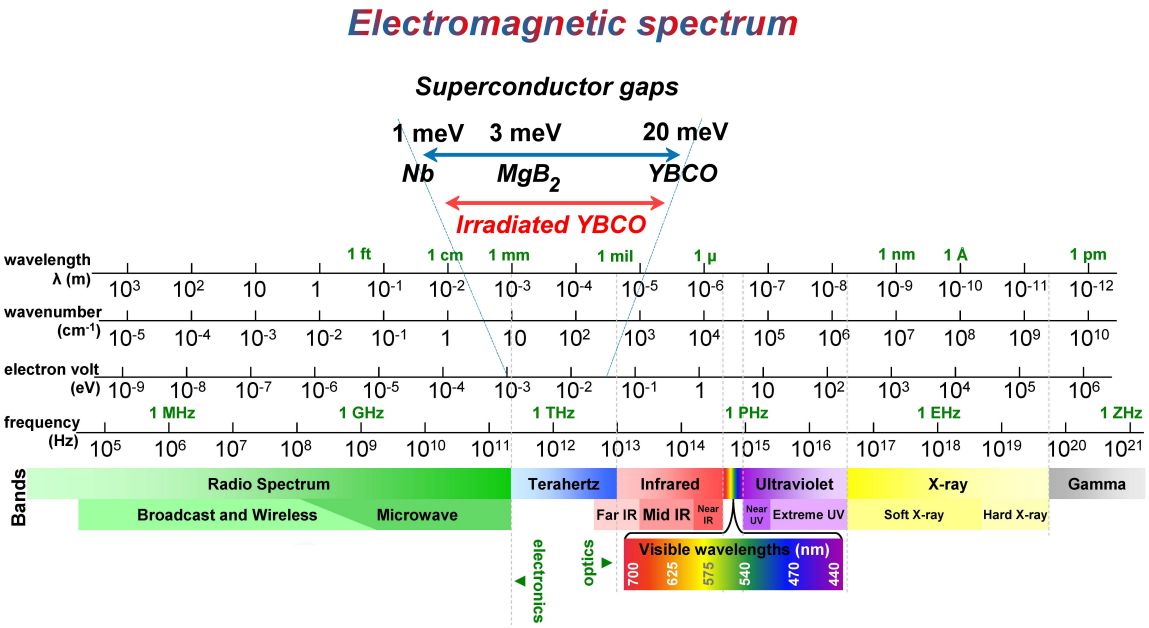

Figure 1.1: Electromagnetic Spectrum (`https://areeweb.polito.it/ricerca/superconductivity/PR/MONADE/index_monade.htm`).

1.1 Evolution of Transmission Spectrum

While sub-6 gigahertz (GHz) and mm-Wave bands have already been implemented in fourth generation (4G) and fifth generation (5G) networks, respectively, the THz and optical frequency bands are the potential candidates for sixth generation (6G) wireless networks [6]. Figure 1.1 demonstrates the electromagnetic spectrum and various frequency bands (such as sub-6GHz, mm-wave, THz, etc.) of wireless networks. In what follows, the explanation for each of them.

1.1.1 Sub-6GHz Spectrum

Sub-6 GHz spectrum is the most commonly used spectrum for cellular communications. Lower frequency transmissions, such as sub-6 GHz transmissions, can propagate further and penetrate through buildings more effectively than higher frequency spectrum, such as mm-wave. However, the sub-6 GHz spectrum is running out of bandwidth to accommodate wireless users. Since the sub-6 GHz spectrum is extremely limited and congested, the achievable data rates can be much lower than those available in the higher spectrum [7]. Two primary factors affect the signal, i.e., large-scale fading created by path loss and shadowing and small-scale fading caused by multi-path propagation. As a result, 5G networks rely on mm-wave spectrum to achieve higher bandwidth and massive connectivity [8].

1.1.2 mm-Wave Spectrum

Mm-wave transmissions (30 - 100 GHz) are identified as a promising technology for future-generation networks to meet the data rate requirements in the order of 10 Gbps [9], [10]. The key benefit of the mm-wave spectrum is its broad bandwidth and smaller form-factor which enables the deployment of massive antennas within a small area, allowing high antenna gain and beamforming to be achieved even in handsets. Unfortunately, since mm-waves experience a higher path-loss than lower frequencies, their range is constrained. Also, since the wavelength is less than a centimetre, mm-wave signals are more vulnerable to environmental attenuation and absorption than sub-6 GHz signals. When mm-wave signals get into contact with large structures, they experience higher diffused scattering than sub-6 GHz signals [11], [12].

1.1.3 THz Spectrum

Following the efficient introduction of mm-wave communications in 5G networks, the research on THz communications is now gaining popularity [13]. THz-band promotes ultra-reliable and low latency applications for multiple indoor scenarios thanks to its broader bandwidth. Also, passive cyber-attacks, such as man-in-the-middle attacks, would be extremely difficult in the THz band [14] because of incredibly short wavelengths and high gain ultra-massive antennas producing extremely focused beams [15, 16]. However, THz signal transmission generates very high losses, undermining the promised benefits, such as reaching a data rate in the order of terabits per second (Tbps).

1.2 Evolution of Multiple Access Schemes

Multiple access, a critical part of wireless networks, has a significant effect on bandwidth usage, system throughput, and latency. Multiple access in cellular radio refers to a technique in which multiple users share a transmission medium to communicate with the wireless access point. Multiple access schemes are instrumental to the performance of wireless networks as they describe how resources (e.g., frequency, time, antennas, power, codes, etc.) should be allocated to users [17]. For example, since bandwidth is typically limited and/or very costly, efficient allocation between users is critical in both the uplink and downlink communications. Typically, when multiple users can access wireless services through their respective dedicated resources, this is referred to as *multiple access*.

Figure 1.2 illustrates the evolution of multiple access schemes with the generations of wireless networks. The multiple access schemes can be classified into two groups,

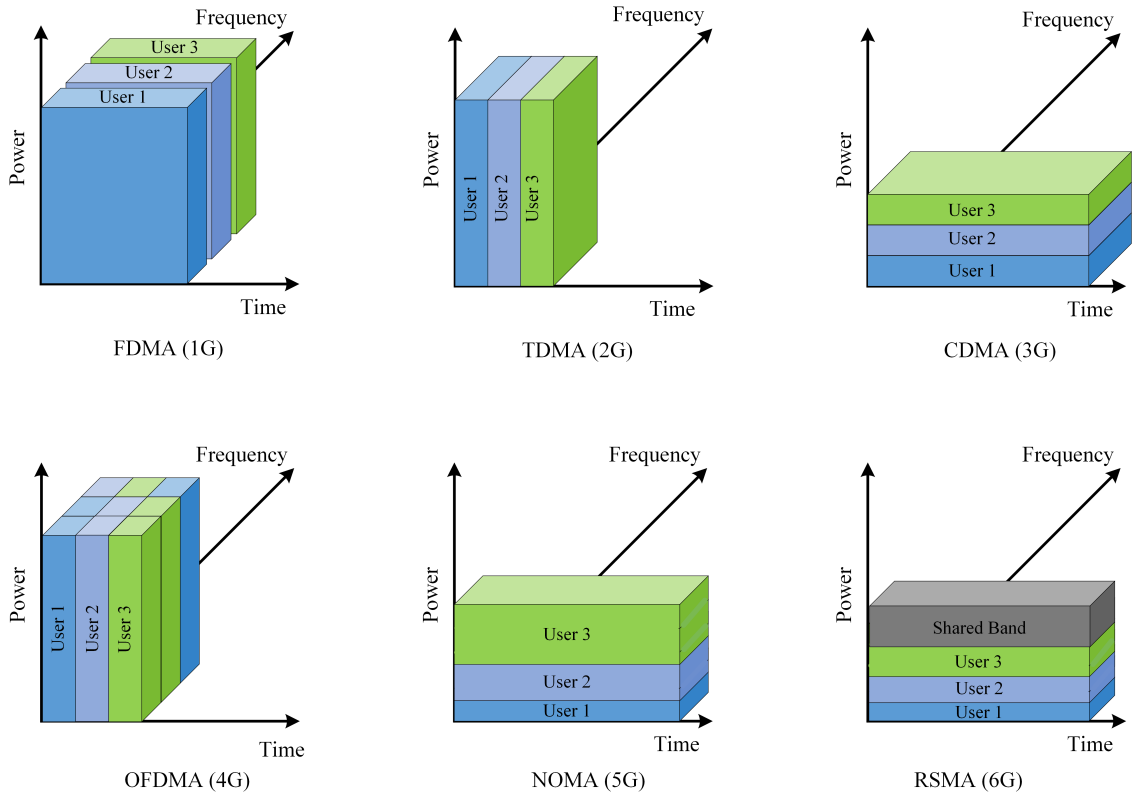

Figure 1.2: Evolution of multiple access schemes over the past decades.

i.e., orthogonal and non-orthogonal multiple access schemes, which are detailed in the subsequent sections.

1.2.1 Orthogonal Multiple Access (OMA)

The users' channel access in OMA is exclusive, i.e., users do not interfere with one another when sharing a networking channel. Due to the orthogonal channel access, there is no inter-user interference. Thus, low-complexity receivers can be used to identify the signal of the intended user. Nevertheless, since the amount of orthogonal resources is restricted, OMA systems cannot support massive connectivity in 5G

and 6G networks. Most common OMA techniques implemented to date in wireless networks are classified as follows:

- **Frequency Division Multiple Access (FDMA):** In FDMA, which has been used in the first generation (1G) of cellular networks, the usable spectrum is divided into non-overlapping frequency sub-bands, each providing one digital data stream [18]. Assigning different channels to the same user is challenging in FDMA since the radios must concurrently demodulate signals from multiple frequency channels. Therefore, FDMA is applicable mainly on analog communication systems, where transmission is continuous, and serves as the basis for the Advance Mobile Phone Service (AMPS) and European Total Access Communication System (ETACS) analog cellular phone standards [19].

- **Time Division Multiple Access (TDMA):** In TDMA, the time resource is split into several time slots, each of which is assigned to users typically in a round-robin manner. TDMA has been utilized in the second generation (2G) of cellular networks [20]. In TDMA, the network dimensions are split into non-overlapping slots along the time axis, and each user is allocated a separate time slot [21]. Since each user in TDMA is assigned a new cyclically repeated time slot, the limitation of TDMA is that the channel features can vary drastically in different slots. As a result, receiver functions that rely on channel estimates, such as equalization, must re-estimate the channel for every period. The Global System for Mobile (GSM), Personal Digital Cellular (PDC), Interim Standard-54 (IS-54), and Interim Standard-136 (IS-136) wireless cellular phone standards utilized TDMA [19].

- **Code Division Multiple Access (CDMA):** uses orthogonal pseudo random

spreading codes to modulate the input signals of various users. The transmitted signals from different users use the same time and bandwidth. CDMA is one example of how user-specific codes scatter the modulated symbol by the processing gain [22] such that the code signatures can be orthogonal to one another. Subsequently, the number of concurrent users that can be assisted is less than or equal to the number of orthogonal codes. The spreading code structure is used by the receiver to distinguish between various users. Third generation (3G) cellular networks were based on a wide-band CDMA standard [23].

- **Orthogonal Frequency Division Multiple Access (OFDMA):** is a multiple access scheme based on the orthogonal frequency-division multiplexing (OFDM) waveform, allowing subcarriers to be packed tightly and orthogonally in the frequency domain with a subcarrier spacing inverse to the symbol length. Furthermore, OFDMA divides the time and frequency plane into two-dimensional resource blocks, each of which can be allocated to a user who transmits a modulated symbol. Orthogonal multiple access based on OFDMA or single carrier frequency-division multiplexing access (SC-FDMA) is used in 4G of cellular networks such as Long-Term Evolution (LTE) and LTE-Advanced, standardized by the third Generation Partnership Project (3GPP) [24].

OMA schemes make it easier to build a transceiver and reduce co-channel interference. These schemes, however, the number of users who may be serviced at the same time is limited. Furthermore, user scheduling and reliable feedback channels are necessary to ensure orthogonality.

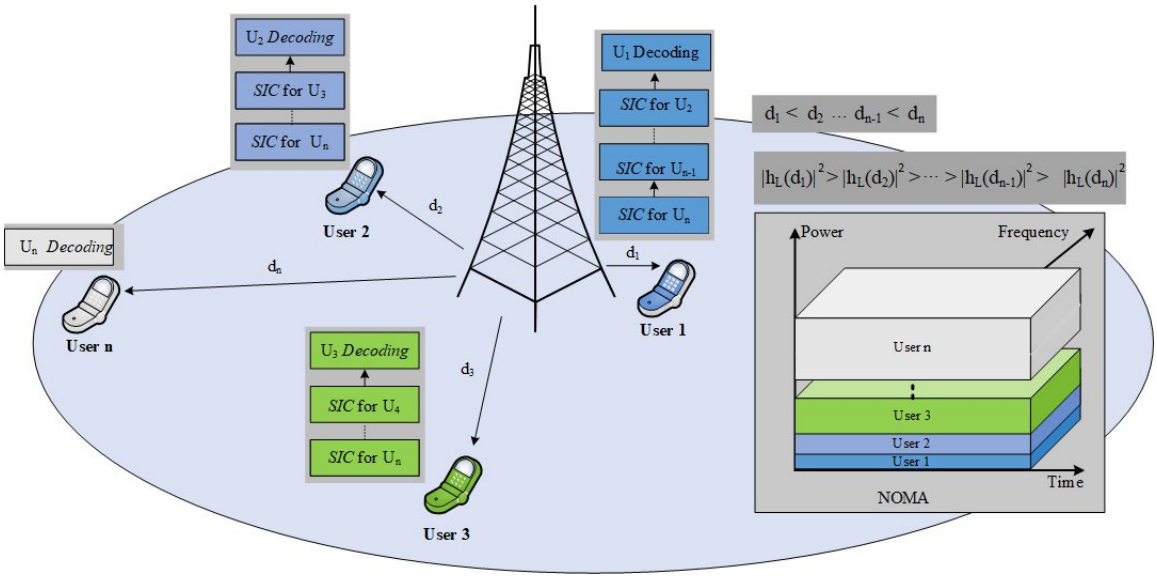

Figure 1.3: Downlink NOMA in a single cell with one AP and n users.

1.2.2 Non-Orthogonal Multiple Access (NOMA)

NOMA is a crucial enabling technology for next-generation wireless networks to attain massive connectivity, higher throughput, and enhanced fairness. NOMA superposes users' message signals in the power domain using linearly precoded superposition coding and leverage on successive interference cancellation (SIC) at the receivers. Figure 1.3 shows the downlink NOMA transmission of a single-antenna access-point (AP) serving n users. In particular, NOMA enables the superposition of various users' message signals on a specific time-frequency resource block [25]. Then, by using SIC, the desired message signal is identified and decoded at the receiver. Some of the primary advantages given by NOMA over OMA include:

- **High Spectral Efficiency:** As NOMA can serve several users within the same time-frequency resource block, it is highly spectrum-efficient given the SIC strategies implemented at the receivers and user pairing performed correctly

[26]. NOMA may also be efficiently combined with other 6G technologies to boost network throughput.

- **Massive Connectivity:** Since the number of users supported by NOMA is not exclusively restricted by the number of available orthogonal time-frequency resources, NOMA can support massive connectivity.

- **Enhanced User Fairness:** The power multiplexing in NOMA enables users' fairness since higher power can be allocated to the cell-edge (poor channel) users; whereas higher data rates can still be ensured as the cell-center (strong channel) users can still receive their transmission with low power allocations. The power allocation in NOMA is more equitable compared to traditional greedy power allocation methods. The authors of [27] proposed fair power allocation processes to enhance higher fairness among users.

- **Low latency:** OMA techniques require an uplink user to submit a scheduling request to the Base-Station (BS) first. In the downlink, the BS then sends a direct signal to the receiver [28]. Therefore, the provisioning mechanism adds latency (with additional signaling overhead), which is undesirable for next-generation communication. On the other hand, grant-free multiple access can be realized in uplink NOMA by automatically identifying active users and decoding their data streams [29]. As a result, the grant-free NOMA has lower latency. Also, note that since many users are served together in NOMA, latency could be reduced.

1.2.3 Rate Splitting Multiple Access (RSMA)

In RSMA schemes, users messages are splitting into common and private parts, where the common parts will be encoded within one or more common streams while the private parts will be encoded into different streams.

User messages are separated to common and private messages at the transmitter. The common messages are merged and encoded to common streams to be decoded by different users. In contrast, private messages are encoded separately into private streams to be decoded by the relevant users only [30]. At the transmitter, all streams are combined and transmitted to the users. Following that, each receiver decodes the common stream(s), conducts SIC, and then decodes its private stream. Thus, each receiver will restore its original message after combining its common and private messages. RSMA can partially decode interference using SIC and partially handle interference as noise, thus allowing for rate and quality of service (QoS) improvements [31]. Figure 1.4 shows the downlink RSMA transmission of a single-antenna AP serving n users. This potential of RSMA to partially mitigate interference and partially address interference as noise enables it to connect the two extremes of completely decoding interference and treating interference as noise, allowing for rate enhancement and complexity reduction [32], [31]. RSMA has a number of benefits to other multiple access schemes, including:

- **Spectral and Energy Efficiency:** Since RSMA is a more general multiple access framework that merges OMA and NOMA as subschemes, it has a higher or equivalent spectral and energy efficiency than existing multiple access strategies. RSMA has been demonstrated to be energy efficient in [33], [34], and [35]

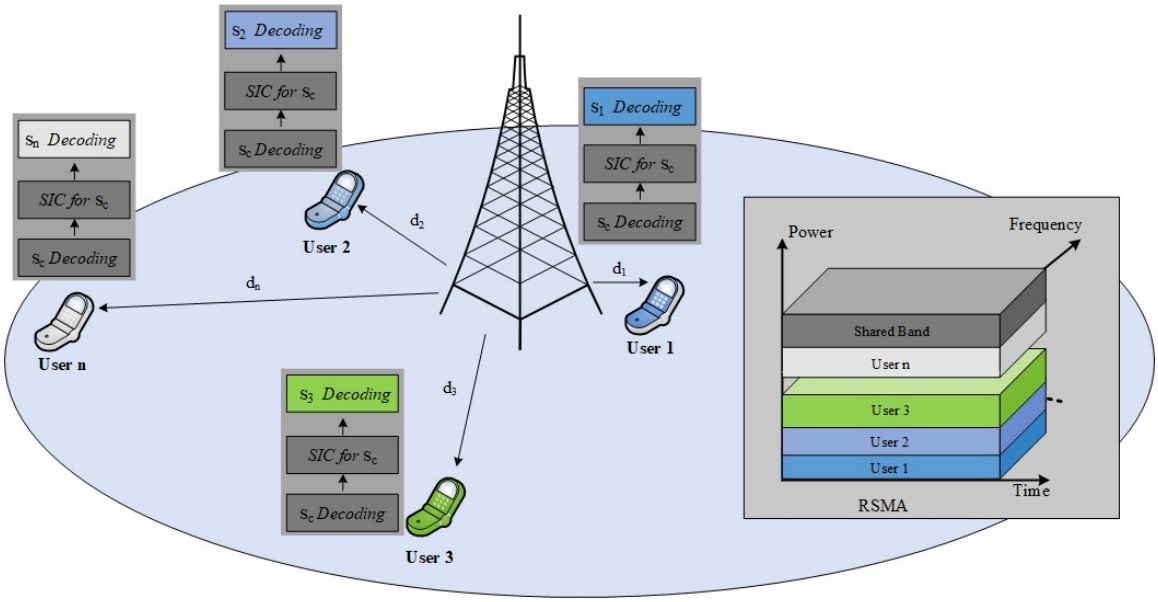

Figure 1.4: Downlink RSMA in a single cell with one AP and n users.

for two users and K users Multi-Input Single-Output (MISO) broadcast channel with varying channel directions and channel strengths, as well as [36] in Unmanned Aerial Vehicles (UAV) networks with fixed and primarily known positions.

- **Flexible:** RSMA is applicable for different types of users (with varying channels, directions, and channel strengths) as well as network loads (underloaded and overloaded regimes). The reason is that RSMA can automatically adapt to alternate multiple access methods, such as spatial division multiple access (SDMA) and NOMA. Also, RSMA can improve interference management by partially decoding the interference and treating the rest as noise.

- **Lower Complexity:** The performance gain of RSMA can be achieved with

lower transmitter and receiver complexity than multi-antenna NOMA. Multi-antenna NOMA, on the other hand, needs user grouping and ordering at the transmit scheduler, as well as numerous levels of SIC at the receivers. RSMA does not need complicated user scheduling and pairing. Subsequently, RSMA can minimize channel state information (CSI) feedback overhead [37], [38].

- **Fairness**: RSMA enables fairness among users by assigning a more considerable weight to a user with poor channel conditions.

1.3 Challenges

Some of the primary challenges of THz networks are listed below:

1.3.1 Molecular Absorption and Propagation Modeling

In the THz bands, there are a variety of path-loss attenuation sources; among which molecular absorption contributes the most to the overall attenuation. Molecular absorption occurs because some energy of THz electromagnetic waves gets absorbed as they migrate the molecules in the transmission medium to higher energy states. Since the THz spectrum has a higher absorption rate, it can experience significant atmospheric attenuation. It may even be absorbed by water vapour, rain, or fog molecules. The attenuation can result in path loss spikes and spectral windows, significantly altering the communication range. As a result, the frequency should be carefully selected to avoid the path loss peaks in the spectrum [39]. Furthermore, the THz channel propagation model leverage on sophisticated Beer's Lambert law to account for the overall path loss and molecular absorption.

1.3.2 Multi-Carrier Transmissions

Multi-carrier transmissions typically divide the overall bandwidth into multiple sub-carriers, with each subcarrier assigned to a single user and each user can have multiple subcarriers. Note that analyzing the performance of multi-carrier NOMA in a conventional sub-6GHz network is straight-forward as all sub-channels experience the identical channel statistics. However, this is not the case in THz networks as the each sub-channel at THz frequencies experience a different molecular absorption coefficient $k_a(f)$. Thus, the channel statistics on each sub-carrier is non-identical as well as frequency dependent, which makes the performance characterization of users in a multi-carrier NOMA network challenging.

1.3.3 User Pairing in THz Network

User grouping in NOMA is one of the fundamental issues and it is necessary to devise conditions for selecting suitable users for NOMA transmissions. While most of the existing literature focuses on greedy user grouping mechanisms where the aggregate throughput of NOMA pair is maximized, it is of paramount importance to derive a fair scheme which groups only users that can benefit from NOMA. Specifically, the question is how to design a user grouping scheme that guarantees the gain of NOMA over OMA for each individual user in that group. Furthermore, in THz networks, adaptive user pairing schemes are crucial where user selection becomes a function of the molecular absorption coefficient which is frequency dependent.

1.4 Contributions

This thesis provides a comprehensive framework to analyze the performance of emerging multiple access schemes (such as NOMA and RSMA) in single carrier and multi-carrier THz networks in the presence of an adaptive user pairing mechanism which not only ensures the gain of NOMA over OMA for all users, but also adapt according to the degree of molecular absorption in THz networks. The primary contributions of the thesis are listed herein:

- I developed a novel low-complexity user pairing scheme in a THz-NOMA network. The proposed scheme ensures NOMA outperform OMA for each individual user in the NOMA pair and adapts according to the molecular absorption.
- I characterized the exact outage probability (OP) expressions in a single-carrier and multi-carrier THz-NOMA network considering Nakagami-m fading to capture the line-of-sight (LoS) feature of THz transmissions, and molecular absorption noise. The derived expressions can be customized for *various user-pairing schemes* and are applicable to the *entire THz frequency range*.
- For multi-carrier THz-NOMA network, I proposed a MGF-based exact approach and derived simplified single integral expressions to compute the OP, as opposed to Fox-H's based expressions in [40].
- The numerical results validated the accuracy of the derived expressions and demonstrated the performance of the proposed user-pairing scheme compared to the conventional random pairing and nearest-farthest schemes.
- I have extended the developed framework to analyze the performance of RSMA

scheme in the downlink transmission of Sub-6 GHz and THz network and the numerical results validated the accuracy of the derived expressions.

1.5 Thesis Outline

The thesis is organized as follows:

- Chapter 2 reviews the essential metrics that can be used to measure the performance of wireless networks and mathematical preliminaries to ensure that the reader has sufficient expertise to follow the discussions and computations in the next chapters. Moreover, I introduced a review of the recent studies to highlight the research gaps in analyzing the performance of emerging multiple access schemes in THz networks.

- Chapter 3 presents a novel framework to derive analytical expressions of the users' performance considering single-carrier and multi-carrier setup in both THz-NOMA and THz-OMA networks. The derived OP expressions are generic in capturing the entire range of THz spectrum, Nakagami-m fading and molecular absorption noise. Furthermore, the adaptive pairing scheme was developed for the THz-NOMA network, where user selection adapts according to molecular absorption, and the gains of NOMA are guaranteed for each individual user.

- Chapter 4 provides a comprehensive framework to analyze the performance of RSMA in the downlink transmission of a single-carrier in sub-6 GHz and THz network. In particular, I characterize OP expressions in the presence of

two different user pairing schemes (benchmarks user-pairing schemes) in Sub-6 GHz-RSMA and THz-RSMA networks considering Nakagami-m fading and molecular absorption noise.

- Chapter 5 presents a brief conclusion and outlines some ideas for possible future directions.

Chapter 2

Mathematical Preliminaries and Literature Review

2.1 Key Performance Indicators

The Signal to Interference Plus Noise Ratio (SINR), data rate and OP are essential metrics that can be used to measure the performance of wireless networks. This section aims to provide a review of these metrics to better understand the performance of wireless communication networks.

2.1.1 Signal to Interference Plus Noise Ratio (SINR)

According to Beer's lambert law, the received signal power at a typical user from the serving THz AP can be stated as follows:

$$S = P\left(\frac{c}{4\pi f d_{(i)}}\right)^2 e^{-k(f)d_{(i)}}\chi_{(i)} = P\zeta d_{(i)}^{-2} e^{-k(f)d_{(i)}}\chi_{(i)}, \tag{2.1}$$

where (i) denotes user i, $k(f)$ is the molecular absorption coefficient, f denotes the THz carrier frequency, c is the speed of light, the channel spreading loss $\zeta = \frac{c}{4\pi f}$, P denotes the total transmit power budget of the AP, $\chi_{(i)}$ is fading channel for user i, and $d_{(i)}$ represents the distance between a typical user and its serving AP. When

two users share the same spectrum, they experience interference I. The SINR at the receiver for a communication channel is thus calculated as follows:

$$\text{SINR} = \frac{S}{I + N}, \tag{2.2}$$

where, N represents the receiver's noise power.

2.1.2 Data Rate

Claude Shannon developed channel capacity in the late 1940s, based on a mathematical theory of communication focused on the idea of mutual information among a channel's input and output [41]. The Shannon–limit theorem indicates the theoretical upper bound (referred to as channel capacity) on the data rate over additive white Gaussian noise (AWGN) channel can be given as:

$$C = B \log_2 (1 + \text{SINR}) = B \log_2 \left(1 + \frac{S}{I + N}\right), \tag{2.3}$$

where the capacity is measured in bits/second (bps), B is the bandwidth of the channel in hertz (Hz), S is the received signal power over the bandwidth measured in watts (or volts squared), N is the power spectral density of the noise, and I denotes the interference over the bandwidth, measured in watts (or volts squared).

2.1.3 Outage Probability (OP)

OP is defined as the probability of not being able to send a signal on a channel successfully. That is, OP is the probability that the SINR of a channel is less than or

equal to some network or users' quality-dependent threshold, i.e.,

$$P_{\text{out}} = P(\text{SINR} < \tau),$$

The coverage probability is therefore defined as the likelihood that the SINR will exceed the threshold, i.e.,

$$P_{\text{cov}} = P(\text{SINR} > \tau) = 1 - P_{\text{out}}$$

2.2 Mathematical Preliminaries

The purpose of providing mathematical preliminaries is to ensure that the reader has sufficient expertise to follow the discussions and computations in the next chapter. Here, I review mathematical preliminaries like ranked random variables, MGF of a random variable, Gil-Pelaez inversion theorem, etc. A more extensive and in-depth discussion of order statistics can be found in [42]. Materials on moments generating functions and characteristic function can be found in [43], Ch.5.7, while the details of Gil-Pelaez Inversion theorem can be found in [44].

2.2.1 Order Statistics

Order statistics can be used to determine the distribution of sorted independent and identically distributed (IID) random variables [42]. For example, the distances between users and an AP can be modeled as IID uniformly distributed random variables $r_1, r_2, \cdots r_N$. The users' distances can then be ordered as $d_1 < d_2 < ... < d_N$, where d_1 and d_N indicate the minimum distance and maximum distance from AP, respectively. Subsequently, the probability density function (PDF) of the distance of user at rank

n can be given as:

$$f_{d_n}(d_n) = \frac{N!}{(n-1)!(N-n)!}(F_r(d_n))^{n-1}(1-F_r(d_n))^{N-n} f_r(d_n), \forall n = 1, ..., N, \quad (2.4)$$

where $f_r(d_n)$ and $F_r(d_n)$ indicate the PDF and the cumulative distribution function (CDF) of user's distances given by the uniform distribution.

2.2.2 Moment-Generating Function (MGF)

To understand MGFs, let's first begin with defining moments. $E[X^n]$ denotes the n-th moment of a random variable X. Other moments, like mean and variance, provide important information about random variables. The expected value $E[X]$ is an example of the first moment. The variance of X is the second central moment. The MGF of a random variable generate all moments and can be defined as follows [43]:

$$M_X(s) = E[e^{-sX}] = \int_{-\infty}^{\infty} e^{-sX} f_X(x)\, dx \quad (2.5)$$

provided this expectation exists for s in some neighborhood of 0. In other words, if there is a positive constant C such that $M_X(s)$ is finite for all $s \in [-C, C]$, we say MGF of X exists. There are two main reasons why the MGF is beneficial. First, the MGF of X provides us with all moments. Second, the MGF uniquely defines the distribution (if one exists). That is, if two random variables have the same MGF, their distributions must be the same. As a result, determining the MGF of a random variable is equivalent to choosing its distribution. We'll see how beneficial this approach is when dealing with sums of independent random variables in next chapter (section 3.4).

2.2.3 Gil-Pelaez Inversion Theorem

In wireless networks, the SINR's CDF is used significantly to determine the OP and coverage probability of a typical user. However, extracting the SINR CDF, which is involved due to the convolution of multiple random variables in the interference expression, is cumbersome. Fortunately, the Gil-Pelaez inversion theorem allows the CDF of the SINR to be computed using characteristic functions (which are connected to MGF of random variables). If there isn't a well-defined MGF for a random variable, we can utilize its characteristic function.

Considering S and I to be independent random variables, and a given SINR threshold τ, the OP of SINR can be formulated as follwos:

$$P_{\text{out}} = Pr\left(\text{SINR} < \tau\right) = Pr\left(\frac{S}{I+N} < \tau\right). \tag{2.6}$$

Let us define a new random variable $X = S - I\tau$, from (2.6) then the OP of SINR can be given as follows:

$$P_{\text{out}} = Pr\left(X = S - I\tau < N\tau\right). \tag{2.7}$$

The equivalent characteristic function of a random variable X can be given as [43]:

$$\Omega_X(\omega) = E[e^{-i\omega X}] = \int_{-\infty}^{\infty} e^{-i\omega X} f_X(x)\, dx, \tag{2.8}$$

where $i = \sqrt{-1}$ and ω is a real number. The CDF of random variable X given its corresponding characteristic function $\Omega_X(\omega)$ can be computed using the Gil-Pelaez

inversion theorem as shown in the following [44]:

$$Q_{\Omega_X(\omega)} = Pr(X < x) = \frac{1}{2} + \frac{1}{\pi}\int_{-\infty}^{\infty} \frac{\mathrm{Im}[\Omega_X(\omega)e^{i\omega X}]}{\omega} d\omega, \tag{2.9}$$

Given that X is a linear combination of independent random variables, the MGF of X can be given as $M_X(i\omega) = E[e^{-i\omega X}] = E[e^{-i\omega(S-I\tau)}]$. Thus, substituting it in the Gil-Pelaez inversion lemma, we can compute the SINR OP as follows:

$$P_{\text{out}} = \frac{1}{2} + \frac{1}{\pi}\int_{0}^{\infty} \frac{\mathrm{Im}[M_X(i\omega)e^{i\omega N\tau}]}{\omega} d\omega, \tag{2.10}$$

2.3 Literature Review

To date, most of the research focused on analyzing the OPs of users in a *single-carrier sub-6GHz* NOMA network [25, 45, 46]. An exception is [40] where the authors considered the OP analysis for multi-carrier NOMA in sub-6GHz or RF networks. The derived expressions rely on approximations and are in the form of Fox H's function. Nevertheless, the performance of NOMA in THz networks is not well-understood neither in single-carrier nor in multi-carrier set-up. Different from RF, the THz transmissions are susceptible to unique challenges such as *molecular absorption noise*[1], *molecular absorption* at different frequencies leading to serious path-loss peaks, and a sophisticated *Beer's Lambert law-based channel* model.

[1]Molecular absorption noise causes signal loss as the electromagnetic (EM) energy gets partially transformed into internal energy of the molecules.

2.3.1 THz-NOMA

Recently, a handful of research works considered analyzing the performance of NOMA in THz networks. For instance, the authors in [47] proposed a THz-NOMA cache-enabled downlink network to maximize energy efficiency, while optimizing user clustering, beamforming, and power allocations. The authors demonstrated that using the suggested enhanced K-means algorithm for user clustering and multipliers' proposed alternating direction approach for power allocation; the proposed network may achieve better energy efficiency. In [48], the authors optimized the transmission powers to maximize energy efficiency in a single carrier THz network. The authors in [49] presented an energy-efficient cooperative NOMA strategy for multi-user indoor THz-MISO systems that assures the minimum required rate for cell-edge users. The potential for increasing the data rates achievable through THz-NOMA was discussed in [50].

Lately, preliminary research demonstrated the gains of NOMA over OMA in THz networks using computer simulations [50]. The authors considered a single THz channel, no fading, random user pairing, and the molecular absorption model was limited to 250 - 450 GHz. In [47], the authors optimized power allocation, user clustering, and hybrid precoding to maximize energy efficiency in a THz-NOMA system. In [51], the authors maximized the network sum-rate while optimizing the beamforming weights, sub-array selection, power allocation, and sub-band assignment in a THz-NOMA network subject to the user's QoS requirements.

2.3.2 RSMA

2.3.2.1 Single Antenna - Optimization

Recently, several existing studies, such as in [52–54], investigated fundamental optimization problems related to RSMA for a single-input-single-output (SISO) system. In [52], the authors introduced a one-dimensional search algorithm for sum-rate maximization considering a SIC constraint to optimize rate allocation and power control in a downlink SISO system for RSMA. Another study in [53] investigated the decoding order and power allocation optimization in an uplink RSMA system. Another research work investigated optimizing the RSMA transmission scheme for a downlink cloud radio access network (C-RAN) in SISO system [54]. The authors presented an efficient RSMA scheme in which each common signal's decoding users have been selected by a hierarchical clustering mechanism based on channel directions.

2.3.2.2 Multi-Antenna - Optimization

Several existing works, such as in [34, 55–58], have recently studied fundamental optimization issues relate to RSMA for a MISO system. In the extension work [55] of [52], the authors proposed a successive convex approximation (SCA)-based algorithm to obtain a locally optimal solution to maximize the network sum rate in MISO RSMA considering the rate and SIC constraints. In [56], the authors suggested a power allocation scheme for multi-user multi-carrier MISO network to maximize the sum-rate of users, considering random beamforming and zero-forcing beamforming for common and private messages. The energy efficiency (EE) maximization problem of RSMA in the MISO broadcast channel has been studied in [34]. The authors obtained optimal EE beamforming using SCA-based approach considering the downlink MISO system

and showed that RSMA is more energy-efficient than SDMA and NOMA. In [57], the authors presented an energy-efficient resource allocation scheme for downlink reconfigurable intelligent surface (RIS)-assisted with RSMA in the MISO system that optimizes the phase shifts of all RISs to maximize the system energy efficiency. In [58], the authors used a modified weighted minimum mean square error (WMMSE) approach jointly with an alternating optimization algorithm to achieve max-min fairness (MMF) in multibeam satellite communications.

2.3.2.3 Outage Analysis

Among the several possible schemes, it has been developed an RSMA scheme in [59] and demonstrated that RSMA is a more generic, reliable, and efficient scheme than SDMA, OMA and NOMA. In contrast to SDMA, which depends on totally treating any residual interference as noise, and NOMA, which depends on fully decoding interference, RSMA has the capacity of partially decoding the interference and partially treating the interference as noise.

In [60], the authors investigated the performance of RSMA in a UAV-BS-assisted multiuser downlink communication system, in which the UAV serviced many users simultaneously through RSMA. They derived closed-form expressions of OP and achievable throughput at each user while considering independent and non-identical Nakagami-m small-scale fading, then used Monte-Carlo simulations to validate the accuracy of the derived analytical expressions.

2.4 Summary

In this chapter, I have provided an overview of the essential metrics that can be used to measure the performance of wireless networks and explained some of the mathematical preliminaries used to compute the performance metrics. Moreover, I presented a review of the recent studies to highlight the research gaps of analyzing the performance of emerging multiple access schemes in THz networks. These gaps are considered and covered in the next two chapters.

Chapter 3

Outage Analysis in Multi-Carrier NOMA-THz Networks

3.1 Motivation/Contribution

To the best of my knowledge, there is no research work that provides a comprehensive framework for the OP analysis of users in a *single-carrier and multi-carrier THz-NOMA* network and/or develops a low-complexity *user pairing scheme* for the THz-NOMA network with a guaranteed gain over OMA for each individual user. It is also noteworthy that analyzing the performance of multi-carrier NOMA in RF networks is straight-forward as all sub-channels experience identical channel statistics. However, in THz networks, each sub-channel experiences a different molecular absorption indicated by its molecular absorption coefficient. Thus the channel statistics on each sub-channel are non-identical. Furthermore, the mathematical structure of the channel propagation model based on Beer's-Lambert law adds to the challenge. Subsequently, characterizing OP expressions in a multi-carrier THz-NOMA network is challenging.

3.2 System model and Assumptions

This proposed framework can be generalized for multiple users by making multiple two-user NOMA pairs in orthogonal time/frequency resource blocks in a straightforward manner. In other words, extending the proposed framework for K users will be possible by considering multiple clusters where each cluster has two users. However, the consideration of other NOMA pairs would not effect the performance of users in a specific NOMA pair, so the study in this chapter is focused on two-user NOMA pair. Note that two-user NOMA has been included in 3GPP LTE-advanced Release-13 as Multiuser Superposition Transmission (MUST) and proved to be beneficial in terms of data rate [61]. NOMA has been studied to increase the spectral efficiency of downlink in the THz network by using superposition coding with SIC. However, considering a framework that has more users in a single NOMA cluster will make it more complex due to the use of SIC, and overheads for synchronization.

In each NOMA cluster that are located at distances d_1 and d_2 from the AP such that $d_1 < d_2$. The users located at d_1 and d_2 are referred to as user 1 (U_1) and user 2 (U_2), respectively. The AP transmits the superposed signal $x = \sqrt{p_1}x_1 + \sqrt{p_2}x_2$ in the downlink, where $x_i, \quad \forall i = 1, 2$ is the unit power message signal of the user i, p_i indicates the total power assigned to the user i. Due to the AP total power limit, $P = \sum_{i=1}^{2} p_i$, the power assigned to a user relies on the powers of other users. The received signal at the ith user before SIC is given by: $y_i = h_i x + \omega_i$ where h_i describes the channel gain between the AP and user i and ω_i represents the additive white Gaussian noise at the receiver for user i (with power spectral density $N_{0,i}$). Consider the message of user u, $\forall u \in \{1, 2\}$, denoted by W_u. Thus, the NOMA transmission model can be illustrated as in Figure 3.2.

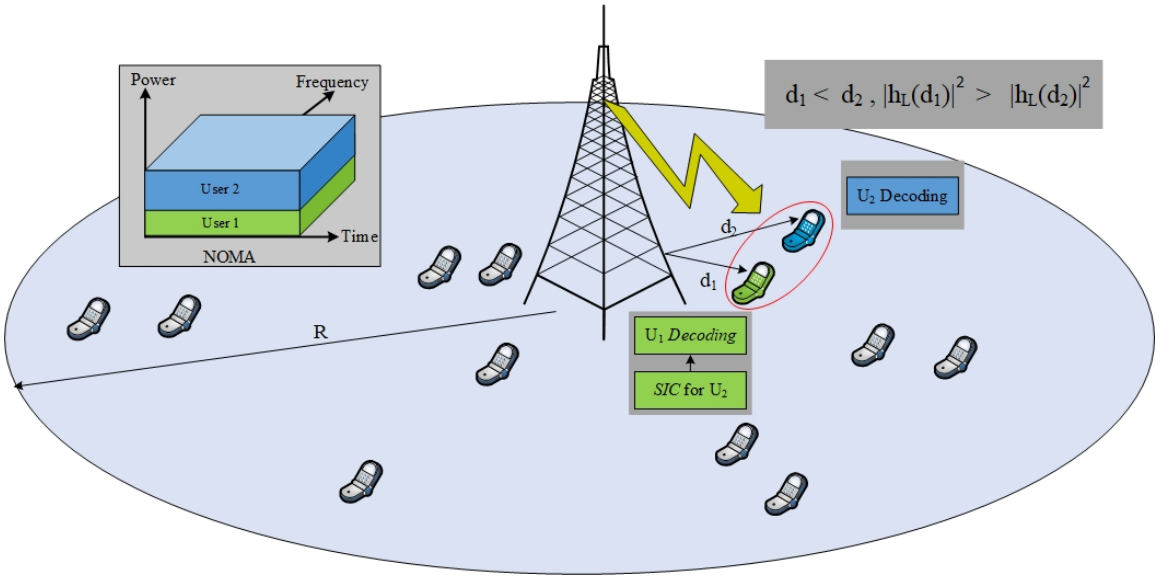

Figure 3.1: Downlink NOMA in a single cell with one AP and 2 users.

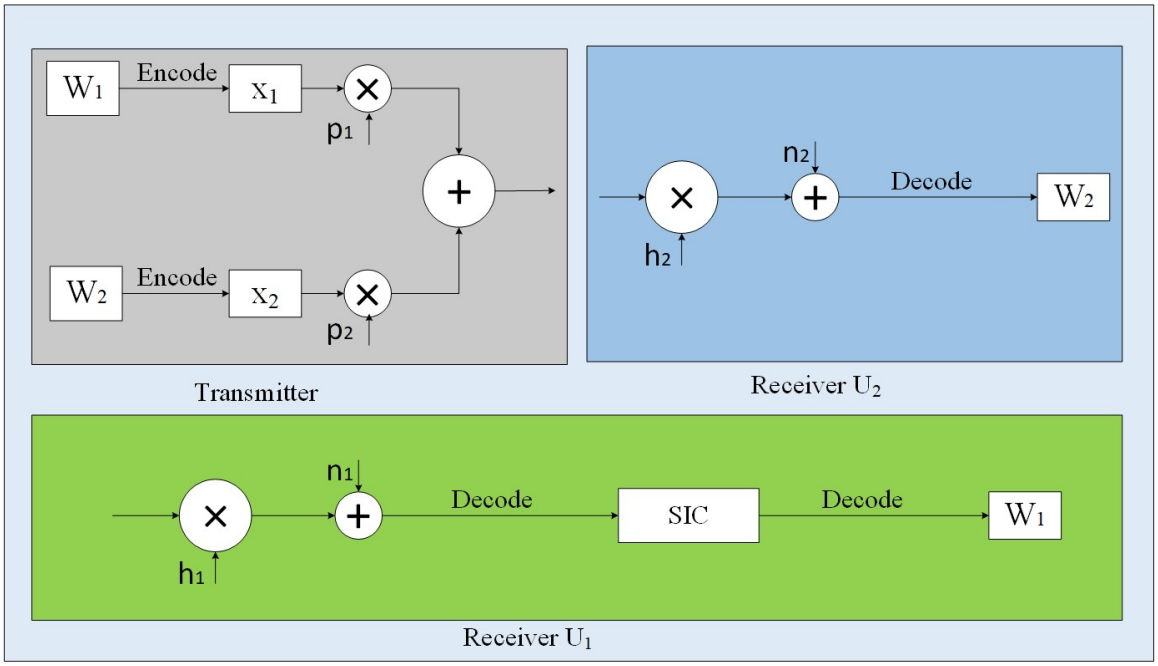

Figure 3.2: Downlink NOMA transmission model

SIC is used to split the signals at the end-users. The superposition coding method is used to multiplex the signals on the transmitter side (the AP) in the downlink situation. The power allocation coefficients for these signals are different. The SIC method is employed on the receiver side to separate interfering signals. Users' channel conditions determine how power allocation coefficients are distributed. Those with poor channel conditions are given more power, whilst users with strong channel conditions are given less power. By considering other signals as interference, the SIC receiver initially decodes the strongest signal as shown in figure 3.1. After this step, the strongest signal is extracted and cancelled from the superposed signal, and the second most powerful signal is decoded and cancelled, so on and so forth, until the poorest signal is decoded.

3.2.1 Molecular Absorption Coefficient

Using radiative transfer theory [62] and HIgh resolution TRANsmission (HITRAN) molecular absorption database [63], the fraction of incident EM radiation at a given frequency that can pass through the medium can be computed using Beer-Lambert Law. This parameter is known as the transmittance of a medium and is given by $\tau(f, d) = e^{-k(f)\ d}$, where f is the EM wave frequency, d represents the transmission distance, and $k(f)$ represents the molecular absorption coefficient which is a function of the frequency and depends on the composition of the medium, i.e., the mixture of molecules in the channel. The absorption loss accounts for the transmission loss induced by the dissipation or transfer of signal energy into the kinetic energy of molecules [64].

The molecular absorption coefficient of the isotopologue i of gas g for a molecular

volumetric density at pressure p and temperature T can be defined as:

$$k(f)=\sum_{(i,g)} \frac{p^2 T_{\mathrm{sp}} q^{(i,g)} N_A S^{(i,g)}}{p_0 T_k V T^2} \; \frac{f \tanh\left(\frac{hcf}{2k_b T}\right)}{f_c^{(i,g)} \tanh\left(\frac{hcf_c^{(i,g)}}{2k_b T}\right)} F^{(i,g)}\left(f\right) \tag{3.1}$$

where p and p_0 indicate the ambient pressure of the transmission medium and the reference pressure [1 atm], respectively, T is the temperature of the transmission medium, T_{sp} stands for the temperature at standard pressure, $q^{(i,g)}$ indicates the mixing ratio of gas, N_A refers to the Avogadro number, and V represents the gas constant. The line intensity $S^{(i,g)}$ defines the strength of the absorption by a specific type of molecules and is directly obtained from the HITRAN database [63]. In addition, f and $f_c^{(i,g)}$ stand for the frequency of the EM wave and the resonant frequency of gas g, respectively, c is the speed of light in the vacuum, h is the Planck's constant, and k_b stands for the Boltzmann constant. The resonant frequency of gas g at reference pressure p_0 is determined as $f_c^{(i,g)} = f_{c_0}^{(i,g)} + \delta^{(i,g)}\left(\frac{p}{p_0}\right)$, where $\delta^{(i,g)}$ is the linear pressure shift [65]. For the frequency band f, I consider the Van Vleck-Weisskopf asymmetric line shape to evaluate the molecular absorption.

$$F^{(i,g)}(f) = \frac{100c\alpha^{(i,g)} f}{\pi f_c^{(i,g)}} \left(\frac{1}{\left(f - f_c^{(i,g)}\right)^2 + (\alpha^{(i,g)})^2} + \frac{1}{\left(f + f_c^{(i,g)}\right)^2 + (\alpha^{(i,g)})^2} \right) \tag{3.2}$$

The absorption from a particular molecule occurs over a range of frequencies and this spreading (if the system pressure is above 0.1 atm) depends on the collisions between molecules of the same gas. This amount of broadening is usually referred to as the

Lorentz half-width $\alpha^{(i,g)}$ defined as follows:

$$\alpha^{(i,g)} = \left(\left(1 - q^{(i,g)}\right)\alpha_{\text{air}}^{(i,g)} + q^{(i,g)}\alpha_0^{(i,g)}\right)\left(\frac{p}{p_0}\right)\left(\frac{T_0}{T}\right)^{\gamma},$$

where T_0 indicates the reference temperature, the parameters air half-widths, $\alpha_{air}^{(i,g)}$, self-broadened half-widths, $\alpha_0^{(i,g)}$, and temperature broadening coefficient,γ, are obtained directly from the HITRAN database [63].

3.2.2 THz LoS Channel Model

The LoS channel transfer function, h_L, is a function of the molecular absorption loss and the spreading loss as shown below:

$$h_L(d_i) = h_S(d_i)h_A(d_i)e^{-2\pi f T_L} \tag{3.3}$$

where the transfer function of the channel spreading loss is defined as: $h_S(d_i) = \frac{c}{4\pi\ f\ d_i}$ where, d_i is the length of the path between the transmitter and the receiver, c is the speed of light, f is the transmitting THz frequency, and $T_L = d_i/c$ is the time period of the LoS propagation. The transfer function of the molecular absorption loss is given by $h_A(d_i) = e^{-0.5k(f)d_i}$. The channel's power gain between the AP and user i is formulated as:

$$|h_L(d_i)|^2 = \left(\frac{c}{4\pi f d_i}\right)^2\ e^{-k(f)d_i} \tag{3.4}$$

3.2.3 Fading Model

I assume the channel fading is Nakagami distributed as it can model a variety of distributions such as Rayleigh fading for non-LoS transmissions and Rician fading

for LoS transmissions, etc. The Nakagami model is suitable because it can describe communication environments with different LoS and non-LoS components using its flexible fading parameter, m [66]. Thus, the power of a Nakagami fading channel follows Gamma distribution whose probability PDF and CDF is shown, respectively, as follows:

$$f_X(x) = \left(\frac{m}{P_r}\right)^m \frac{x^{m-1}}{\Gamma(m)} e^{(\frac{-mx}{P_r})} \tag{3.5}$$

$$F_X(x) = \frac{\gamma(m, \frac{P_r x}{m})}{\Gamma(m)} \tag{3.6}$$

where m is the fading severity parameter. The Nakagami distribution becomes Rayleigh fading when $m = 1$ and it can model Rician fading when $m = (K + 1)^2/(2K + 1)$, where K is the ratio of the power in the LoS part to the power in the different multipath elements (non-LoS). Additionally, there's no fading observed when $m \to \infty$ and worst fading when $m = 0.5$.

3.2.4 Antenna Model

Consider THz AP and users devices are equipped with directional antennas with sectorized gain patterns as in [67], [68], and [69] to approximate the actual antenna pattern. The sectorized gain pattern is given by:

$$G_q(\theta) = \begin{cases} G^q_{\max} & \mid \theta \mid \leq w_q \\ G^q_{\min} & \text{otherwise,} \end{cases} \tag{3.7}$$

where q subscript denotes transmitter and receivers devices, respectively, $q \in \{\mathrm{t}, \mathrm{r}\}$, $\theta \in [-\pi, \pi)$ is the angle of the boresight direction, w_q is the main lobe beamwidth, $G^q_{\max}$ is the main lobe antenna gain,and $G^q_{\min}$ is the side lobe antenna gain. Beam

alignment strategies are used to align the user and the desired THz AP so that their main lobes overlap.

3.2.5 SINR - NOMA Model

The SINR for U_1 and U_2 can be given, with perfect successive-interference cancellation are modeled, respectively, as follows:

$$\mathrm{SINR}_1^{(\mathrm{noma})} = \frac{a_1 G_t G_r P |h_L(d_1)|^2 \chi_1}{N_1^{\mathrm{noma}}} \tag{3.8}$$

$$\mathrm{SINR}_2^{(\mathrm{noma})} = \frac{a_2 G_t G_r P |h_L(d_2)|^2 \chi_2}{a_1 G_t G_r P |h_L(d_2)|^2 \chi_2 + N_2^{\mathrm{noma}}} \tag{3.9}$$

where χ follows Nakagami-distributed fading channel, and G_t and G_r are the directional antenna gains of the THz AP and users. Beam alignment strategies are assumed that align the main lobes of the users and the THz AP. The noise at the receivers of U_1 and U_2 comprises of thermal noise and molecular absorption noise as defined, respectively, below:

$$N_1^{(\mathrm{noma})} = k_b T + a_1 \zeta P d_1^{-2} (1 - e^{-k_a(f) d_1}) \chi_1 \tag{3.10}$$

and

$$\begin{aligned} N_2^{(\mathrm{noma})} &= k_b T + (a_1 + a_2) \zeta P d_2^{-2} (1 - e^{-k_a(f) d_2}) \chi_2 \\ &= k_b T + \zeta P d_2^{-2} (1 - e^{-k_a(f) d_2}) \chi_2 \end{aligned} \tag{3.11}$$

where a_1 and a_2 depict the portion of the AP transmit power allocated for U_1 and U_2 such that $a_1 + a_2 = 1$. Also, P denotes the total transmit power budget at

AP. Since without loss of generality the channel gains are assumed to be ordered as $h_L(d_1)\chi_1 > h_L(d_2)\chi_2$, take $a_1 < a_2$ which enables U_2 to detect its own signal without performing SIC. The interference observed at U_2 due to the signal of U_1 is weak for two reasons: (i) low transmit power allocated for the message signal of U_1, and (ii) the poor channel gain of U_2. On the other hand, U_1 detects its own signal after canceling the interference from U_2. The spectral efficiency of transmission in NOMA to U_1 and U_2 can thus be computed for a duration of time $\hat{T}$ as

$$\mathrm{C_i^{(noma)}} = \hat{T}\log_2(1+\mathrm{SINR}_i), \quad \forall i = \{1,2\}.$$

3.2.6 SINR - OMA Model

Similarly, the SINR for U_1 and U_2 in OMA model, where each user receives their downlink transmission for a predefined duration of $\hat{T}/2$, is modeled as follows:

$$\mathrm{SINR}_i^{(\mathrm{oma})} = \frac{G_t G_r P|h_L(d_i)|^2\chi_i}{N_i^{(\mathrm{oma})}}, \quad \forall i = \{1,2\}, \tag{3.12}$$

where the noise can be calculated in OMA for U_1 and U_2 as

$$N_i^{(\mathrm{oma})} = N_0 + G_t G_r \zeta P d_i^{-2}\left(1 - e^{-k(f)d_i}\right)\chi_i, \quad \forall i = \{1,2\}.$$

Thus, the spectral efficiency of transmission in OMA to U_1 and U_2 can be computed as

$$\mathrm{C}_i^{(\mathrm{oma})} = \frac{\hat{T}}{2}\log_2\Big(1+\mathrm{SINR}_i^{(\mathrm{oma})}\Big), \quad \forall i = \{1,2\}.$$

Without loss of generality, the duration $\hat{T}$ is taken as unity.

3.3 Outage Analysis: Single-Carrier THz-NOMA

In this section, I first describe the proposed user-pairing scheme along with the two benchmark user-pairing schemes, describe the distance distributions of the users, and present a framework to calculate the OP of users for the proposed and benchmark user-pairing schemes.

For bench-marking purposes, I consider a random and nearest-farthest user pairing scheme. In the random pairing scheme, I pick only two users randomly with independent and identically distributed distances r_1 and r_2 from AP. The near and far user's distance can thus be defined as $d_1 = \min(r_1, r_2)$ and $d_2 = \max(r_1, r_2)$, respectively. Therefore, the PDF and CDF of the distances of U_1 and U_2 are given, respectively, as follows:

$$f_{d_1}(d_1) = 2f_r\left(d_1\right)\left(1 - F_r\left(d_1\right)\right), \quad F_{d_1}(d_1) = 1 - \left[1 - F_r\left(d_1\right)\right]^2, \tag{3.13}$$

$$f_{d_2}(d_2) = 2f_r\left(d_2\right)F_r\left(d_2\right), \quad F_{d_2}\left(d_2\right) = \left[F_r\left(d_2\right)\right]^2. \tag{3.14}$$

On the other hand, in the nearest-farthest scheme, I select two users out of N users with minimum and maximum distances from the AP. The near and far user's distance can thus be defined as $d_1 = \min(r_1, r_2, \cdots, r_N)$ and $d_2 = \max(r_1, r_2, \cdots, r_N)$, respectively. The PDF and CDF of d_1 and d_2 can thus be given, respectively, as follows:

$$f_{d_1}(d_1) = N[1 - F_r\left(d_1\right)]^{N-1} f_r\left(d_1\right), \quad F_{d_1}(d_1) = 1 - \left[1 - F_r\left(d_1\right)\right]^N \tag{3.15}$$

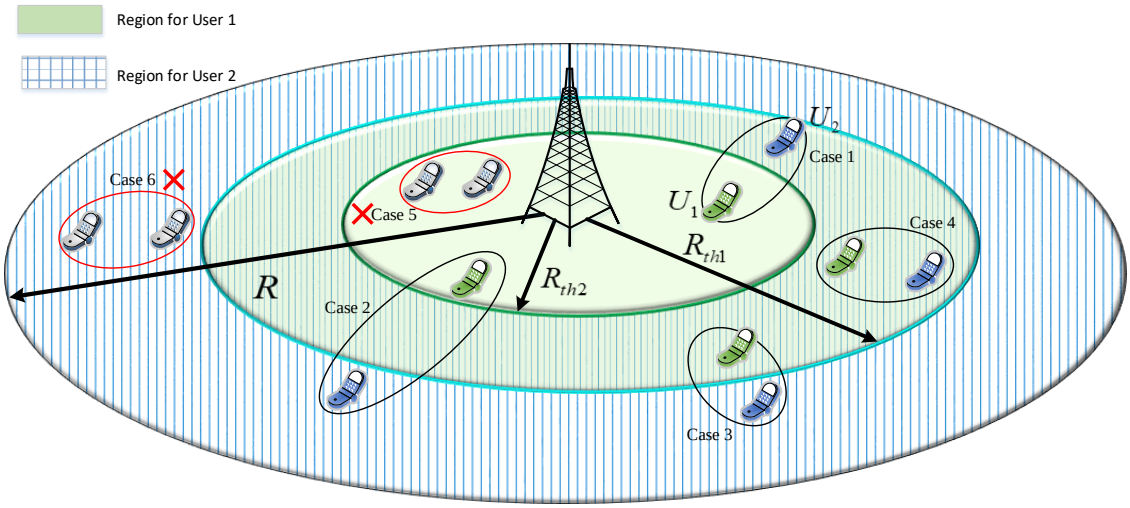

Figure 3.3: User grouping scheme based on $\mathrm{R_{thr_1}}$ and $\mathrm{R_{thr_2}}$.

$$f_{d_2}(d_2) = N\left[F_r(d_2)\right]^{N-1} f_r(d_2), \quad F_{d_2}(d_2) = \left[F_r(d_2)\right]^N, \tag{3.16}$$

where the PDF and CDF of r are given, respectively, as $f_r(r) = \frac{2r}{R^2}$, $F_r(r) = \frac{r^2}{R^2}$, since all users are uniformly distributed in a circular region of radius R.

3.3.1 Proposed User Grouping Scheme

Different from the conventional approach where user-pairing is typically performed to maximize the sum-rate performance of users in a NOMA pair, the proposed user scheme selects only those users who can benefit from NOMA transmissions compared to OMA transmission. The contribution related to the proposed user pairing is that the proposed scheme enables fairness among users by allowing each of them to join a NOMA pair if and only if they have a benefit over OMA. Certainly, the proposed scheme ensures the performance benefits of each user in a NOMA pair. To ensure the gains of NOMA over OMA for each user, the proposed scheme applies the *necessary*

conditions in which NOMA outperforms OMA, i.e., I use the conditions $d_1 < d_2$ and $C_i^{(\text{noma})} > C_i^{(\text{oma})}$, $\forall i = \{1, 2\}$ resulting in the following.

Lemma 1 (Proposed User Pairing Scheme)**.** *The proposed pairing scheme is a sufficient condition for NOMA to outperform OMA, where the near user should be within the distance R_{th1} and the far user should be located beyond the distance R_{th2}, such that $d_1 < d_2$, where:*

$$R_{\text{th1}} = \frac{1}{k(f)} \ln\left(\frac{1 - a_1}{1 - 2a_1}\right), \tag{3.17}$$

and

$$R_{\text{th2}} = \frac{1}{k(f)} \ln\left(\frac{{a_1}^2}{1 - 2a_1} + 1\right). \tag{3.18}$$

Comparing (3.17) to (3.18), it is straight-forward to verify that $R_{\text{th1}} > R_{\text{th2}}$ always, since $a_1 + a_2 = 1$.

Evidently, as can also be seen in figure 3.3, four user-pairing cases are possible to guarantee the gains of NOMA over OMA for each individual user. The three regions can vary as a function of $k(f)$ and the allocated powers a_1, a_2, e.g., increasing a_1 will increase both R_{th1} and R_{th2}. However, increasing $k(f)$ will decrease both R_{th1} and R_{th2}. This is different from RF NOMA, wherein there is only one case possible due to only one threshold distance (or two regions).

Lemma 2. *The PDF and CDF of d_1 and d_2 in the proposed scheme are given, respectively, as follows:*

$$f_{d_1}(d_1) = \frac{2d_1}{R_{\text{th1}}^2}, F_{d_1}(d_1) = \frac{d_1^2}{R_{\text{th1}}^2}, \tag{3.19}$$

$$f_{d_2}(d_2) = \frac{2d_2}{R^2 - R_{\text{th2}}^2}, F_{d_2}(d_2) = \frac{d_2^2 - R_{\text{th2}}^2}{R^2 - R_{\text{th2}}^2}. \tag{3.20}$$

Corollary 1 (Enhanced Proposed Scheme)**.** *The proposed scheme can be enhanced further in terms of spectral efficiency by selecting the nearest user as* U_1*. In this case,* $f_{d_1}(d_1)$ *and* $F_{d_1}(d_1)$ *can be given as in* (3.15)*.*

3.3.2 OP Analysis

The OP is defined as the probability that user i does not achieve its target-spectral efficiency τ_i, i.e.,

$$\mathcal{O}_i^{(\cdot)} = \Pr\left(\mathrm{C}_\mathrm{i}^{(\cdot)} \leq \ \tau_i\right), \tag{3.21}$$

where $(\cdot)$ denotes NOMA or OMA transmission. Now I formally derive the OP of users in NOMA and OMA separately.

3.3.2.1 Near User (U_1)

The OP of the near user in the downlink NOMA mode is given as:

$$\begin{aligned}\mathcal{O}_1^{(\mathrm{noma})} &= \Pr\left(\frac{B_1 d_1^{-2} e^{-k_a(f)d_1}\chi_1}{N_0 + B_1 d_1^{-2}\left(1-e^{-k(f)d_1}\right)\chi_1} \leq \ y_1\right) \\ &= \int_0^R \frac{\gamma\left[m, \frac{y_1 N_0 d_1^2}{\Theta B_1\left(e^{-k(f)d_1}(1+y_1)-y_1\right)}\right]}{\Gamma(m)} f_{d_1}(d_1)\, dd_1, \end{aligned} \tag{3.22}$$

where $\gamma(\cdot)$ is the lower incomplete Gamma function, $\Gamma(\cdot)$ is the complete Gamma function, m is the fading severity, Θ is the fading power, $y_1 = 2^{\tau_1} - 1$ and $B_1 = a_1 G_t G_r P \zeta$. Since the thermal noise N_0 is negligible compared to the molecular absorption noise in THz networks, (3.22) is simplified as:

$$\hat{\mathcal{O}}_1^{(\mathrm{noma})} = 1 - \Pr\left(d_1 \leq \frac{\ln\left(\frac{1+y_1}{y_1}\right)}{k\left(f\right)}\right) = 1 - F_{d_1}\left(\frac{\ln\left(\frac{1+y_1}{y_1}\right)}{k\left(f\right)}\right). \tag{3.23}$$

Now substituting (3.13) in (3.23) or (3.22) for random scheme, (3.15) in (3.23) or (3.22) for nearest-farthest scheme, and (3.19) in (3.23) or (3.22) for proposed scheme, gives us the OP expressions. The OP of U_1 in the proposed scheme is given as:

$$\hat{\mathcal{O}}_1^{(\text{noma})} = 1 - \left(\frac{\ln\left(\frac{1+y_1}{y_1}\right)}{R_{\text{th1}}\, k\,(f)} \right)^2. \tag{3.24}$$

The OPs of near user in the downlink OMA with and without noise can be given by replacing B_1 with $A = G_t G_r P \zeta$ and y_1 with $x = 2^{2\tau_1} - 1$ in (3.22), (3.23), and (3.24) for all schemes.

3.3.2.2 Far User (U_2)

The OP of the far user in the downlink NOMA mode is formulated as follows:

$$\begin{aligned} \mathcal{O}_2^{(\text{noma})} &= \Pr\left(\frac{B_2 |h_L(d_2)|^2 \chi_2}{B_1 |h_L(d_2)|^2 \chi_2 + N_2^{(\text{noma})}} \leq y_2 \right) \\ &= \int_0^R \frac{\gamma\left[m,\ \frac{y_2 N_0 d_2^2}{\Theta\left(e^{-k_a(f) d_2} (B_2 \ + \ y_2 B_2) - y_2 \ (B_1 + B_2) \ \right)} \right]}{\Gamma(m)} f_{d_2}(d_2)\, dd_2, \end{aligned} \tag{3.25}$$

where, $B_2 = (a_1 + a_2) G_t G_r P$. Ignoring the thermal noise N_0, (3.25) can be simplified as follows:

$$\hat{\mathcal{O}}_2^{(\text{noma})} = 1 - F_{d_2}\left(\frac{\ln\left[\frac{a_2 + a_2 y_2}{y_2}\right]}{k\,(f)} \right). \tag{3.26}$$

Now substituting (3.14) in (3.26) for random scheme, (3.16) in (3.26) for nearest-farthest, and (3.20) in (3.26) for proposed scheme, gives us the OP expressions. The

OP of the far user in the proposed scheme is given as:

$$\hat{\mathcal{O}}_2^{(\text{noma})} = 1 - \frac{\left(\frac{\ln\left[\frac{a_2+a_2y_2}{y_2}\right]}{k(f)}\right)^2 - R_{\text{th2}}^2}{R^2 - R_{\text{th2}}^2}. \tag{3.27}$$

The OPs of the far user in the downlink OMA can be given by replacing d_1 with d_2, B_1 with $A = G_t G_r P \zeta$ and y_2 with $x = 2^{2\tau_2} - 1$ in (3.22), (3.23), and (3.24) for all schemes.

3.4 Outage Analysis: Multi-Carrier THz-NOMA

In this section, I present MGF-based approach to derive tractable outage expressions of the users in a multi-carrier THz-NOMA network. Both the near and far users will get N subcarriers allocated. The spectral efficiency of U_1 and U_2 is given, respectively, as:

$$C_1^{(\text{noma})} = \sum_{n=1}^{N} \log_2\left(1 + \frac{B_1 \chi_{1,n} d_1^{-2} e^{-k_a(f_n)d_1}}{N_{1,n}^{(\text{noma})}}\right), \tag{3.28}$$

$$C_2^{(\text{noma})} = \sum_{n=1}^{N} \log_2\left(1 + \frac{B_2 \chi_{2,n} d_2^{-2} e^{-k(f_n)d_2}}{B_1 \chi_{2,n} d_2^{-2} e^{-k(f_n)d_2} + N_{2,n}^{(\text{noma})}}\right). \tag{3.29}$$

The OP can thus be formulated as follows:

$$\begin{aligned}\mathcal{O}_i^{(\text{noma})} &= \Pr\left(C_i^{(\text{noma})} < \tau_i\right) = \Pr\left(\sum_{n=1}^{N} \log_2(W_{i,n}) < \tau_i\right), \\ &= \Pr\left(X_i = \sum_{n=1}^{N} \ln(W_{i,n}) < \tau_i \ln(2)\right).\end{aligned} \tag{3.30}$$

Note that the MGF is a useful tool to deal with the sum of random variables. For instance, characterizing the PDF becomes analytically intractable for a sum of random variables due to multiple convolutions required. On the other hand, the MGF of a sum of random variables can be derived by deriving the product of the MGF of all random variables. Therefore, to analyze the OP of users in a multi-carrier THz-NOMA network, I resort to an MGF-based approach. The methodology is as follows: **(i)** I first derive the PDF of $W_{i,n}$ conditional on d_1 for near user and d_2 for far user, **(ii)** derive the conditional MGF of $X_{i,n} = \ln W_{i,n}$, **(iii)** compute the conditional cumulative MGF of $X_i = \sum_{n=1}^{N} \ln W_{i,n}$, i.e., $M_{X_i|d_i} = \prod_{n=1}^{N} M_{X_{i,n}|d_i}$, and **(iv)** substitute in the Gil-Pelaez inversion lemma to compute the OP as follows:

$$\mathcal{O}_i^{(\text{noma})} = \frac{1}{2} + \frac{1}{\pi} \int_0^{\infty} \frac{\text{Im}[M_{X_i}(s) e^{j\omega\tau_i \ln(2)}]}{\omega} d\omega, \tag{3.31}$$

where $s = j\omega$, $M_{X_i}(s) = \mathbb{E}_{d_i}[\prod_{n=1}^{N} M_{X_{i,n}|d_i}]$, and

$$\begin{aligned} M_{X_{i,n}|d_i}(s) &= E[e^{-s \ln(W_{i,n})}|d_i] = E[{W_{i,n}}^{-s}|d_i], \\ &= \int_{-\infty}^{\infty} {W_{i,n}}^{-s} f_{W_{i,n}}(W_{i,n})\, dW_{i,n}. \end{aligned} \tag{3.32}$$

From (3.28) and (3.29), I have the following:

$$\chi_{1,n} = g_1(W_{1,n}) = \frac{N_0(W_{1,n} - 1)}{W_{1,n}\left(e^{-k(f)d_1} - 1\right) B_1 d_1^{-2} + B_1 d_1^{-2}},$$

$$\chi_{2,n} = g_2(W_{2,n}) = \frac{N_0 - N_0 W_{2,n}}{B_2 d_2^{-2}(W_{2,n} - a_2 e^{-k_a(f)d_2}\ W_{2,n} - 1)}.$$

Since χ is Gamma distributed, I apply random variable transformation to get the

PDF of $W_{1,n}$ and $W_{2,n}$ as:

$$f_{W_{1,n}}\left(W_{1,n}\right)=\frac{B_1 d_1^{-2}\left(W_{1,n}\left(e^{-k(f)d_1}-1\right)+1\right)^2}{N_0 e^{-k(f)d_1}}\left(\frac{\chi_{1,n}^{m-1}e^{\frac{-\chi_{1,n}}{\Theta}}}{\Theta^m\Gamma\left(m\right)}\right)\Bigg|_{\chi_{1,n}=g_1(W_{1,n})} \tag{3.33}$$

and

$$f_{W_{2,n}}\left(W_{2,n}\right)=\frac{B_2 d_2^{-2}\left(W_{2,n}(a_2 e^{-k_a(f)d_2}-1)+1\right)^2}{a_2 N_0 e^{-k(f)d_2}}\left(\frac{\chi_{2,n}^{m-1}e^{\frac{-\chi_{2,n}}{\Theta}}}{\Theta^m\Gamma\left(m\right)}\right)\Bigg|_{\chi_{2,n}=g_2(W_{2,n})} \tag{3.34}$$

respectively. Finally, I can obtain $M_{X_{1,n}}(s)$ and $M_{X_{2,n}}(s)$ by substituting (3.33) in (3.32) and (3.34) in (3.32), respectively.

Lemma 3. *For enhanced tractability, I ignore the thermal noise and obtain the following simplified results.*

$$W_{1,n}=\frac{1}{1-e^{-k(f)d_1}}\quad\text{or}\quad d_1=\frac{1}{k\left(f\right)}\ln\left[\frac{W_{1,n}}{W_{1,n}-1}\right],$$

$$W_{2,n}=\frac{1}{1-a_2e^{-k(f)d_2}}\quad\text{or}\quad d_2=\frac{1}{k\left(f\right)}\ln\left[\frac{a_2W_{2,n}}{W_{2,n}-1}\right].$$

Subsequently, the outage can be computed by following on the fact that X_i is a constant conditional on d_i and the CDF of a constant is a unit-step function. Subsequently, I have:

$$\begin{aligned}\mathcal{O}_i^{(\text{noma})}&=\Pr\left(X_i=\sum_{n=1}^{N}\ln(W_{i,n})<\tau_i\ln(2)\right)\\&=\int_0^R\mathbb{U}(X_i-\tau_i\ln(2))f_{d_i}(d_i)dd_i.\end{aligned} \tag{3.35}$$

Now substituting (3.13) *in* (3.35) *for random scheme and* (3.15) *in* (3.35) *for nearest-farthest scheme gives the respective OPs.*

From (3.17), I note that the R_{th1} and R_{th2} will vary for each carrier, since they depend on the frequency-dependent absorption coefficient $k(f)$ which is computed using. Thus, each carrier should be allocated to a user selected from a different region based on the proposed scheme. Therefore, I extended the proposed scheme for multi-carrier networks by choosing a user from a region that is valid for all subcarriers.

Corollary 2. *Consider* $R_{\text{th1}}^{\min} = \min(R_{\text{th}_\text{n}}), \forall n \in \{1, 2, \cdots, N\}$ *and* $R_{\text{th2}}^{\max} = \max(R_{\text{th}_\text{n}}), \forall n \in \{1, 2, \cdots, N\}$ *for near user and far user, respectively. Subsequently, after applying* $R_{\text{th1}}^{\min}$ *and* $R_{\text{th2}}^{\max}$*, the PDF of the distance of near user and far user can be given, respectively, as follows:*

$$f_{d_1}(d_1) = \frac{2d_1}{R_{\text{th1}}^{\min}}, \quad f_{d_2}(d_2) = \frac{2d_2}{R^2 - R_{\text{th2}}^{\max}}. \tag{3.36}$$

Now substituting (3.36) in (3.35) for the proposed scheme gives the outage expressions of users in our proposed scheme.

3.5 Numerical Results and Discussions

In this section, I compare the performance of U_1 and U_2 in a single-carrier and multi-carrier THz-NOMA network considering a variety of user-pairing schemes (i) random scheme, (ii) proposed scheme, (iii) enhanced scheme, and (iv) near-far user pairing schemes.

Unless stated otherwise, the parameters are listed herein. I consider 300 users are uniformly distributed in a circular disc of radius 60 m. The antenna gains G_t and G_r

Table 3.1: Simulation Parameters for Calculating $k(f)$ in (3.1)

Symbol	**Value**	**Symbol**	**Value**
p_0, p	1 atm, 1 atm	$q^{(i,g)}$	0.05 [%]
T_0, T	296 K, 396 K	k_b	1.3806×10^{-23} J/K
$f_{c_0}^{(i,g)}$	276 Hz	T_{sp}	273.15 K
γ	0.83	N_A	6.0221×10^{23}
$S^{(i,g)}$	2.66^{-25}Hz-m^2/mol	h	6.6262×10^{-34} J s
$\alpha_0^{(i,g)}, \alpha_{\text{air}}^{(i,g)}$	0.916Hz, 0.1117Hz	c	2.9979×10^{8} m/s
$\delta^{(i,g)}$	0.0251 Hz	V	8.2051×10^{-5}m^{3}atm/K/mol

are set as 20 dB. The AP transmit power is 1W and the power allocation coefficients $a_1 = 0.33$ and $a_2 = 1 - a_1$. Note that our framework is general for any arbitrary value of a_1 in the range $0 \leq a_1 < 0.5$. Nakagami-m fading parameter is set as 2 and $\Omega = 1$. In multi-carrier NOMA, I consider six subcarriers, where each subcarrier has the same transmission bandwidth, with the frequencies [0.85, 0.9, 0.95, 1.0, 1.05, 1.1] THz and their respective $k(f)$ =[0.0357, 0.04, 0.0446, 0.0494, 0.0545, 0.0598] m^{-1} computed using (3.1) considering water vapour molecules. I list the numerical values of parameters in **Table 3.1** which are taken from [70].

Figure 3.4 depicts the OP of U_1 and U_2 for different values of $k(f)$ and validates (3.22) and (3.25) through Monte-Carlo simulations. It is shown that the values obtained through derived expressions (shown in circles), exactly match those obtained through simulations (shown by lines). The enhanced scheme (Corollary 1) significantly outperforms the random and nearest-farthest schemes. It is interesting to note that our scheme adapts user selection based on the molecular absorption coefficient $k(f)$. That is, R_{th1} and R_{th2} reduce with the increase in $k(f)$ as can be seen from (3.17) and (3.18), respectively. Thus, closeby users are selected to combat the effect of increased molecular absorption. Finally, it can be seen that the OP increases with

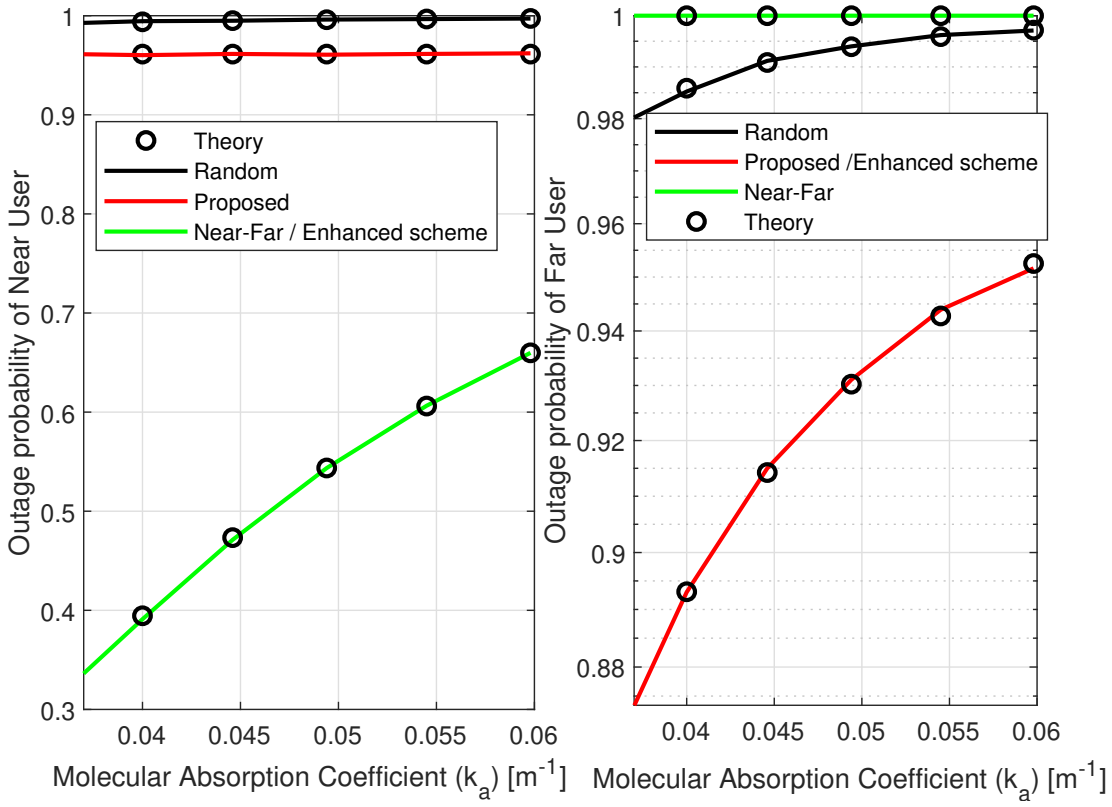

Figure 3.4: Outage performance of near and far users as a function of the molecular absorption coefficient in THz spectrum considering a single-carrier network, $R = 60$ m, $\tau_1 = 3$ bps/Hz, and $\tau_2 = 0.5$ bps/Hz.

the increase in frequency and $k(f)$ due to increased molecular absorption; therefore, a lower THz frequency with lower $k(f)$ is preferred.

Figure 3.5 demonstrates the OP of U_1 and U_2 as a function of the power allocation coefficient of near user (a_1) and highlights the gain of NOMA over OMA. With the increase in a_1, the OP at U_2 increases due to the increased interference from U_1 and increasing values of R_{th2} as can be seen in (3.18). On the other hand, with the increase in a_1, the OP at U_1 increases due to the increasing values of R_{th1} as can be seen in

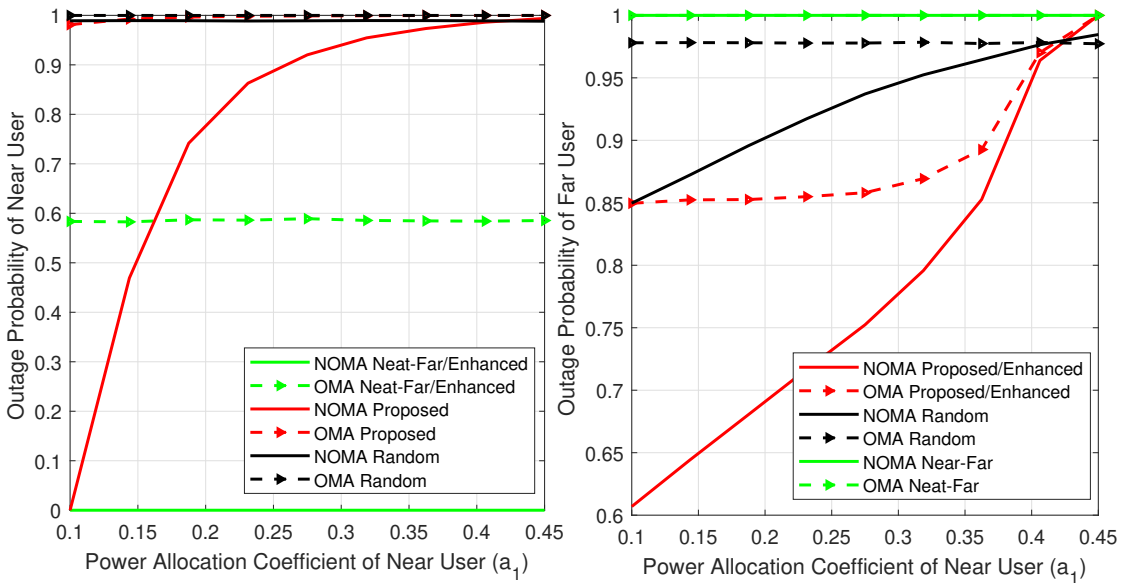

Figure 3.5: Outage performance of near and far users as a function of the power allocation coefficient of near user considering a single-carrier network, $k(f) = 0.03$ $R = 60$ m, $\tau_1 = 3$ bps/Hz and $\tau_2 = 0.5$ bps/Hz.

(3.17). Our scheme adapts the user pairing according to the change in a_1. The gain of NOMA over OMA improves for low values of a_1 and is significant for the enhanced and proposed schemes. Besides, I can observe that NOMA's performance gets close to OMA's when a_1 is close to 0.5.

Figure 3.6 shows the OP of U_1 and U_2 as a function of the number of channels for different schemes in a multi-carrier network. The OP decreases significantly when the number of channels allocated to the user increases due to aggregate spectral efficiency. I note that the increase in subchannels benefits the near user more as the outage decreases exponentially; whereas, the outage decreases linearly for the far user due to its channel conditions. Our analytical results match well with the simulations, and it is evident that the enhanced scheme outperforms benchmark schemes for both

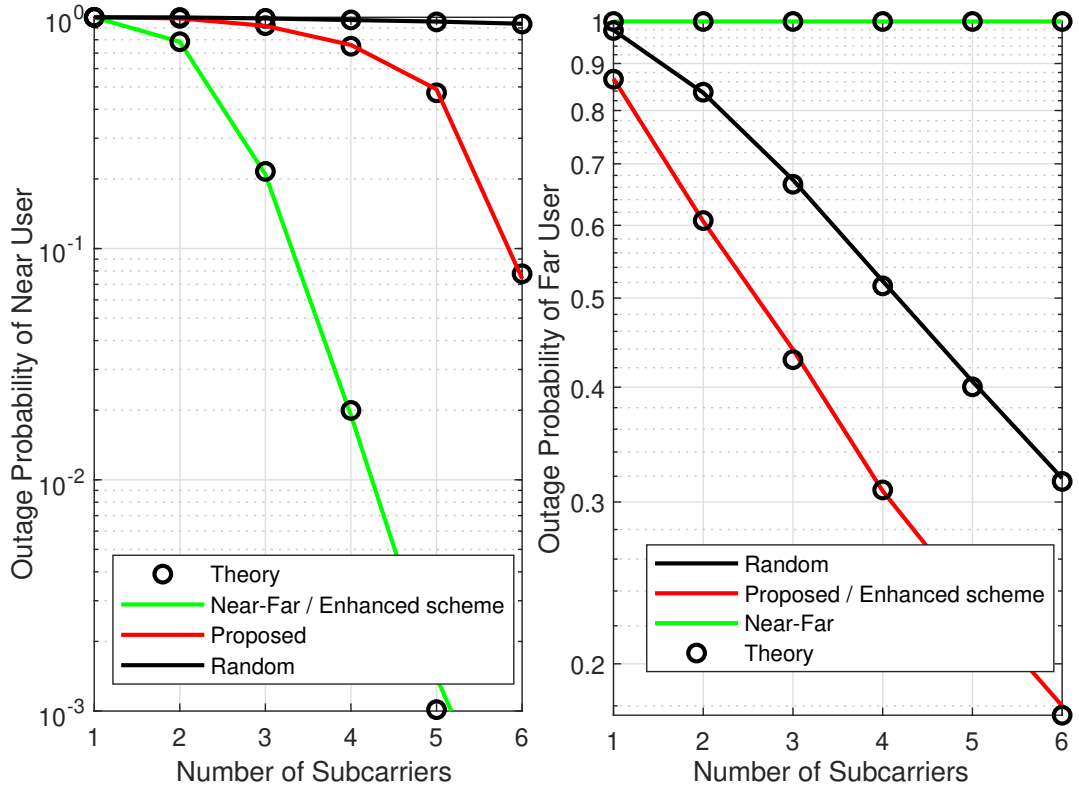

Figure 3.6: Outage performance of near and far users as a function of the number of subcarriers in THz spectrum, τ_1=8 bps/Hz and τ_2=0.5 bps/Hz.

users.

3.6 Summary

In this research work, I analyzed the performance of users considering single-carrier and multi-carrier set-up in both THz-NOMA and THz-OMA networks. The derived OP expressions are general to capture the entire range of THz spectrum, Nakagami-m fading and molecular absorption noise. I have developed an adaptive pairing scheme

for the THz-NOMA network where user selection adapts according to molecular absorption, and the gains of NOMA are guaranteed for each individual user. The framework can be extended to analyze the diversity order or optimize network parameters, e.g., transmit power allocations.

Chapter 4

Outage Analysis in RSMA Networks

4.1 Motivation/Contribution

This chapter provides a comprehensive framework to analyze the performance of rate splitting multiple access (RSMA) in the downlink transmission of a single-carrier in sub-6GHz and THz network. In particular, I characterize OP expressions in the presence of various user pairing schemes, Nakagami-m channel fading, and molecular absorption noise. Numerical results validate the accuracy of the derived expressions.

To achieve the optimal QoS for 6G cellular networks, it is important to incorporate certain sophisticated multiple access schemes, such as RSMA. The use and efficiency of RSMA in THz wireless networks must be studied further to utilize their full potential. Furthermore, to the best of my knowledge, there is no research work that provides a comprehensive framework for the OP analysis of users in Sub-6GHz based-RSMA and THz-RSMA networks. As a result, in this chapter I investigate the efficiency of a single-carrier in the Sub-GHz and THz band that uses RSMA to serve two users at the same time. I evaluated network performance in particular by evaluating the closed-form expression of the achievable potential at each user.

In the sequel, the main contributions of this chapter include:

- I characterize the exact OP expressions in Sub-6GHz-RSMA and THz-RSMA networks considering Nakagami-m fading to capture line-of-sight environment, and molecular absorption noise.
- The expressions can be customized for *benchmarks user-pairing schemes* and are applicable to the *entire frequency range* for both RF-RSMA and THz-RSMA network.
- The numerical results validate the accuracy of the derived expressions.

4.2 System Model and Assumptions

Consider a RSMA-based downlink transmission from an AP to two users, as shown in figure 4.1. The AP is equipped with a single antenna while serving two users with single-antenna for each, U_1 and U_2. The message of user u, $\forall u \in \{1, 2\}$, denoted by W_u, is divided into common parts $W_{u,c}$ and a private part $W_{u,p}$. The common parts are combined and encoded together to form one common stream, denoted by s_c. And, s_u is the private stream of the encoded private message $W_{u,p}$, $\forall u \in \{1, 2\}$. Figure 4.2 shows RSMA transmission model. The resulting streams are then assigned precoding weights and superposed for transmission, assuming that the AP has perfect channel knowledge. Hence, the received signal at user u can be expressed by

$$y_u = h_u x + n_u, \quad \forall u \in \{1, 2\}, \tag{4.1}$$

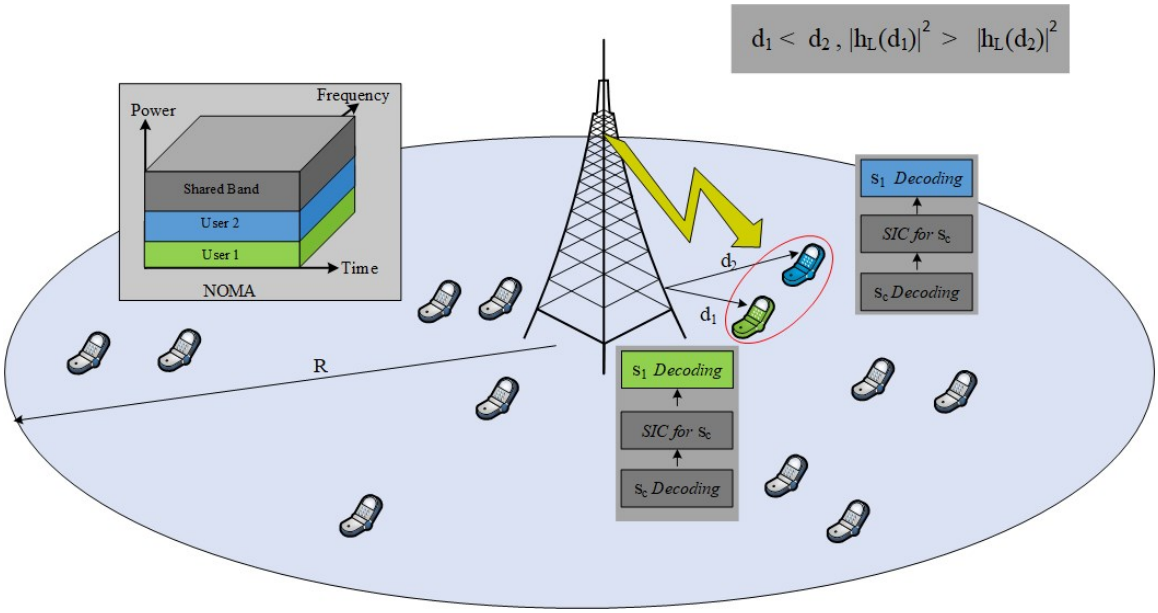

Figure 4.1: Downlink RSMA in a single cell with one AP and 2 users.

where n_u is the complex additive white Gaussian noise (AWGN) with zero-mean and variance σ^2, x is the transmit signal which can be expressed as follows:

$$x = \mathbf{ps},$$

where, $\mathbf{s} = [s_c, s_1, s_2]^T$ is the transmitted signal vector, $\mathbf{p} = [p_c, p_1, p_2]$ is the precoding vector or power vector, and h_u is the channel gain from the AP to user u, and assumed to be perfectly known at the transmitter.

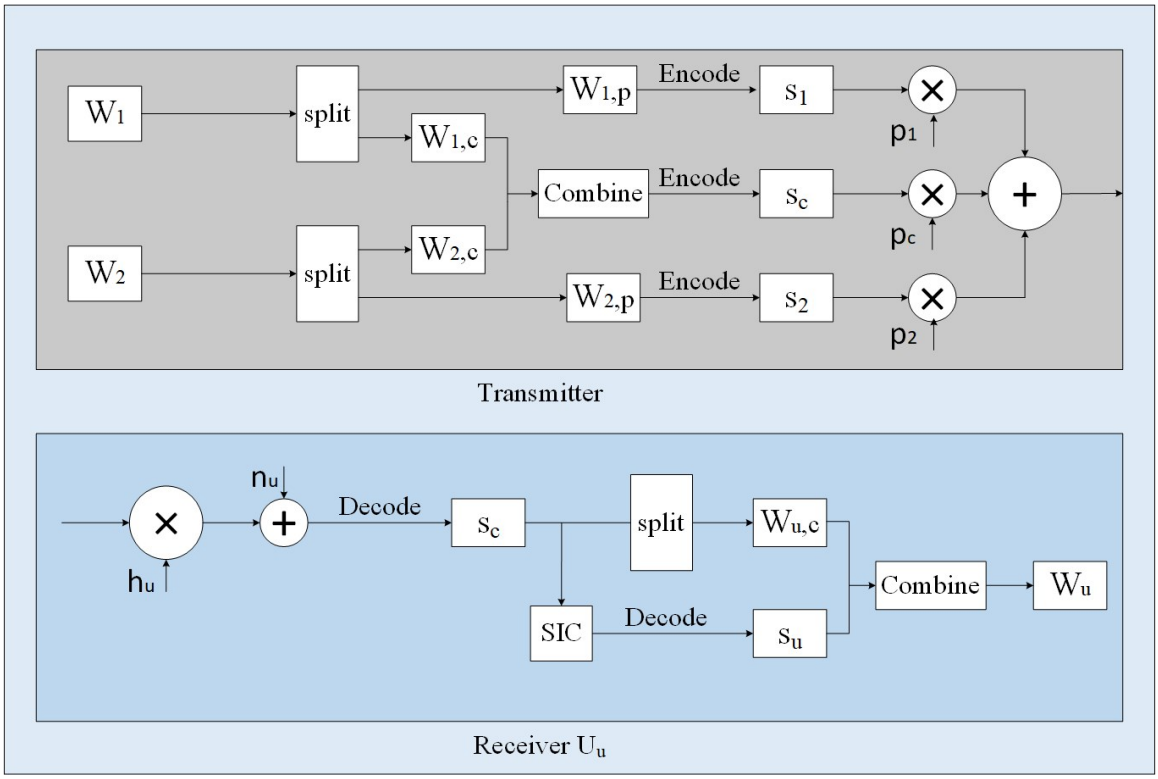

Figure 4.2: Downlink RSMA transmission model.

4.2.1 Channel Model

The line-of-sight (LoS) channel power between the AP and user u in THz netowrk is formulated as follows:

$$h_u^{\text{THz}} = \left(\frac{c}{4\pi f d_u}\right)^2 e^{-k_a(f)d_u} = \zeta d_u^{-2} e^{-k_a(f)d_u}, \quad \forall u \in \{1,2\}, \tag{4.2}$$

where, d_u represents the transmission distance from AP to user u, f is the transmitting carrier frequency, ζ represents the transfer function of the channel spreading loss and defined as $\zeta = \left(\frac{c}{4\pi f}\right)^2$, and $k_a(f)$ is the molecular absorption coefficient defined in

section 3.2.1. The LoS channel power between the AP and user u in RF is given as:

$$h_u^{\mathrm{RF}} = \left(\frac{c}{4\pi f}\right)^2 d_u^{-\alpha}, \quad \forall u \in \{1,2\}, \tag{4.3}$$

where α denotes the path-loss exponent. At user u, the signal s_c is decoded first, while the rest of the signals are considered to be noise. Then, the common message signal is subtracted from the original signal using SIC. Finally, s_u is decoded, $\forall u \in \{1,2\}$.

4.2.2 SINR Model: Common message

The SINRs for the common parts of U_1 and U_2 with perfect SIC are modeled as:

$$\gamma_u^c = \frac{G_t G_r p_c h_u \chi_u}{G_t G_r p_1 h_u \chi_u + G_t G_r p_2 h_u \chi_u + N_u^{\mathrm{com}}}, \quad \forall u \in \{1,2\}, \tag{4.4}$$

where χ is Nakagami-m fading channel, G_t and G_r are the directional antenna gains of the AP and users, respectively. p_1, p_2, and p_c depict the AP transmit power allocated for U_1 and U_2, respectively, such that $p_1 + p_2 + p_c = p$, where, p denotes the total transmit power budget of the AP. Beam alignment strategies are assumed that align the main lobes of the users and the THz AP. The noise at the receivers of U_1 and U_2 comprises of thermal noise N_0 and molecular absorption noise as defined below:

$$\begin{aligned} N_u^{\mathrm{com}} &= k_b T + G_t G_r (p_1 + p_2 + p_c) \zeta d_u^{-2} (1 - e^{-k(f) d_u}) \chi_u, \quad \forall u \in \{1,2\}, \\ &= k_b T + \zeta d_2^{-2} (1 - e^{-k(f) d_u}) \chi_u, \quad \forall u \in \{1,2\}, \end{aligned} \tag{4.5}$$

where, T is the temperature of the channel and k_b is the Boltzmann constant.

4.2.3 SINR Model: Private Messages

The SINRs for the private messages of U_1 and U_2 with perfect SIC are modeled as

$$\gamma_1^{\mathrm{pr}} = \frac{G_t G_r p_1 h_1 \chi_1}{G_t G_r p_2 h_1 \chi_1 + N_1^{\mathrm{pr}}}, \tag{4.6}$$

and

$$\gamma_2^{\mathrm{pr}} = \frac{G_t G_r p_2 h_2 \chi_2}{G_t G_r p_1 h_2 \chi_2 + N_2^{\mathrm{pr}}}. \tag{4.7}$$

The noise at the receivers of U_1 and U_2 comprises of thermal noise N_0 and molecular absorption noise as defined below:

$$N_u^{\mathrm{pr}} = k_b T + G_t G_r (p_1 + p_2) \zeta d_u^{-2} (1 - e^{-k(f) d_u}) \chi_u, \quad \forall u \in \{1, 2\}. \tag{4.8}$$

4.2.4 Data Rate

The corresponding data rates of U_1 and U_2 (in bps/Hz) for common and private messages are given, respectively, as follows:

$$R_u^c = B \ \log_2(1 + \gamma_u^c), \quad \forall u \in \{1, 2\}, \tag{4.9}$$

and

$$R_u^{\mathrm{pr}} = B \ \log_2(1 + \gamma_u^{\mathrm{pr}}), \quad \forall u \in \{1, 2\} \tag{4.10}$$

where B is the channel bandwidth. To decode the common stream s_c at both users, the common rate shall not exceed the minimum of common decoded signals, i.e.,

$$R^{\mathrm{com}} = \min\{R_1^c, R_2^c\},$$

This common data rate R^{com} is then shared between users, where C_u^{com} is user u's portion of the common rate with

$$R^{\text{com}} = C_1^{\text{com}} + C_2^{\text{com}}. \tag{4.11}$$

Consequently, the total data rate of user u, denoted by R_u^{tot}, can be expressed by

$$R_u^{\text{tot}} = C_u^{\text{com}} + R_u^{\text{pr}}, \quad \forall u \in \{1, 2\}. \tag{4.12}$$

4.3 General Outage Analysis: RSMA

Considering $C_{\text{th,u}}$ is the desired data rate threshold for the common message and $R_{\text{th,u}}$ is the desired data rate of the private message for user u, we define the OP for user u as follows:

$$\mathcal{O}_u^{\text{rsma}} = \Pr(C_u^{\text{com}} \leq C_{\text{th}}) \Pr(R_u^{\text{pr}} \leq R_{\text{th}}), \quad \forall u = \{1, 2\}, \tag{4.13}$$

Using (4.10), I can rewrite the private part of (4.13) as follows:

$$\Pr(R_u^{\text{pr}} \leq R_{\text{th}}) = \Pr(\gamma_u^{\text{pr}} \leq \gamma_{\text{th}}^{\text{pr}}), \quad \forall u = \{1, 2\}, \tag{4.14}$$

where $\gamma_{\text{th}}^{\text{pr}} = 2^{\frac{\text{R}_{\text{th}}}{\text{B}}} - 1$. Now substituting (4.6) in (4.14) or (4.7) in (4.14) gives us the outage expression of the private messages of U_1 and U_2, respectively, as follows:

$$\Pr\left(\gamma_1^{\text{pr}} \leq \gamma_{\text{th}}^{\text{pr}}\right) = \Pr\left(h_1 \leq \frac{\gamma_{\text{th}}^{\text{pr}} \sigma^2}{p_1 - \gamma_{\text{th}}^{\text{pr}} p_2}\right) \tag{4.15}$$

and

$$\Pr\left(\gamma_2^{\rm pr} \leq \gamma_{\rm th}^{\rm pr}\right) = \Pr\left(h_2 \leq \frac{\gamma_{\rm th}^{\rm pr}\sigma^2}{p_2 - \gamma_{\rm th}^{\rm pr} p_1}\right) \tag{4.16}$$

Wehre $\sigma^2 = \frac{1}{G_t G_r \zeta}$, Note that the data rate of the common message depends on the minimum of common decoded signals. Using (4.11), I can rewrite the common part of (4.13) as follows:

$$\Pr(C_u^{\rm com} \leq C_{\rm th}) = \Pr(R^{\rm com} \leq C_{\rm th} + C_{u'}^{\rm com}), \quad \forall u = \{1,2\}, \forall u' = \{2,1\}, \tag{4.17}$$

Without loss of generality, I consider the common rate is equal for both users (i.e., $C_1^{\rm com} = C_2^{\rm com}$), and the channel gains are sorted in ascending order, i.e., $h_1 \geq h_2$. To ensure that all both users can successfully decode the common stream, the rate of common stream should be as:

$$\min\{R_1^c, R_2^c\} = R_2^c = B\ \log_2(1+\gamma_2^c), \tag{4.18}$$

then OP for common message at U_1 and U_2 can be written as:

$$\begin{aligned}\Pr(C_u^{\rm com} \leq C_{\rm th}) &= \Pr\left(\frac{R^{\rm com}}{2} \leq C_{\rm th}\right), \quad \forall u = \{1,2\} \\ &= \Pr(\min\{R_1^c, R_2^c\} \leq 2C_{\rm th}) \\ &= \Pr(R_2^{\rm c} \leq 2C_{\rm th}).\end{aligned} \tag{4.19}$$

In the following, $\Pr(R_2^{\rm c} \leq 2C_{\rm th})$ using (4.9) can be given as follows:

$$\Pr(R_2^{\rm c} \leq 2C_{\rm th}) = \Pr\left(\gamma_2^c \leq \gamma_{\rm th}^{\rm com}\right), \tag{4.20}$$

where, $\gamma_{\text{th}}^{\text{com}} = 2^{\frac{2C_{\text{th}}}{B}} - 1$. Now substituting (4.4) in (4.20) we get:

$$\Pr(\gamma_2^c \leq \gamma_{\text{th}}^{com}) = \Pr\left(h_2 \leq \frac{\gamma_{\text{th}}^{\text{com}}\sigma^2}{p_c - \gamma_{\text{th}}^{\text{com}}(p_1 + p_2)}\right). \tag{4.21}$$

4.4 Outage Analysis: RSMA-RF Network

4.4.1 Near User

Calling (4.15) for the private message of near user in RF network, the OP can be formulated as follows:

$$\Pr\left(\gamma_1^{\text{pr}} \leq \gamma_{\text{th}}^{\text{pr}}\right) = \Pr\left(h_1^{\text{RF}} \leq \frac{\gamma_{\text{th}}^{\text{pr}}\sigma^2}{p_1 - \gamma_{\text{th}}^{\text{pr}}p_2}\right) \tag{4.22}$$

By substituting (4.3) in (4.22), then (4.22) is simplified as:

$$\begin{aligned}\Pr\left(\gamma_1^{\text{pr}} \leq \gamma_{\text{th}}^{\text{pr}}\right) &= \Pr\left(d_1 \geq \left(\frac{\gamma_{\text{th}}^{\text{pr}}\sigma^2}{p_1 - \gamma_{\text{th}}^{\text{pr}}p_2}\right)^{-\frac{1}{\alpha}}\right) \\ &= 1 - F_{d_1}\left[\left(\frac{\gamma_{\text{th}}^{\text{pr}}\sigma^2}{p_1 - \gamma_{\text{th}}^{\text{pr}}p_2}\right)^{-\frac{1}{\alpha}}\right]\end{aligned} \tag{4.23}$$

Now substituting (3.13) in (4.23) for random scheme, and (3.15) in (4.23) for nearest-farthest scheme, gives us the OP for the private message part, i.e.,

$$\text{Random}: \qquad \Pr\left(\gamma_1^{\text{pr}} \leq \gamma_{\text{th}}^{\text{pr}}\right) = \left[1 - \frac{1}{R^2}\left(\frac{\gamma_{\text{th}}^{\text{pr}}\sigma^2}{(p_1 - \gamma_{\text{th}}^{\text{pr}}p_2)}\right)^{-\frac{2}{\alpha}}\right]^2 \tag{4.24}$$

$$\text{Nearest} - \text{Farthest}: \qquad \Pr\left(\gamma_1^{\text{pr}} \leq \gamma_{\text{th}}^{\text{pr}}\right) = \left[1 - \frac{1}{R^2}\left(\frac{\gamma_{\text{th}}^{\text{pr}}\sigma^2}{(p_1 - \gamma_{\text{th}}^{\text{pr}}p_2)}\right)^{-\frac{2}{\alpha}}\right]^N \tag{4.25}$$

Now, by calling (4.19) and given that $\Pr(C_u^{\text{com}} \leq C_{\text{th}}) = \Pr(R_2^{\text{c}} \leq 2C_{\text{th}}) = \Pr\left(\gamma_2^c \leq \gamma_{\text{th}}^{\text{com}}\right)$ where, $\gamma_{\text{th}}^{\text{com}} = 2^{\frac{2C_{\text{th}}}{B}} - 1$, we can calculate:

$$\begin{aligned}
\Pr(C_u^{\text{com}} \leq C_{\text{th}}) &= 1 - \Pr\left(\gamma_2^c \geq \gamma_{\text{th}}^{\text{com}}\right) \\
&= 1 - \Pr\left(h_2 \geq \frac{\gamma_{\text{th}}^{\text{com}}\sigma^2}{p_c - \gamma_{\text{th}}^{\text{com}}(p_1 + p_2)}\right) \\
&= 1 - \Pr\left(d_2 \leq \left(\frac{\gamma_{\text{th}}^{\text{com}}\sigma^2}{p_c - \gamma_{\text{th}}^{\text{com}}(p_1 + p_2)}\right)^{-\frac{1}{\alpha}}\right) \\
&= 1 - F_{d_2}\left[\left(\frac{\gamma_{\text{th}}^{\text{com}}\sigma^2}{p_c - \gamma_{\text{th}}^{\text{com}}(p_1 + p_2)}\right)^{-\frac{1}{\alpha}}\right]. \qquad (4.26)
\end{aligned}$$

Now substituting (3.13) in (4.26) for random scheme, and (3.15) in (4.26) for nearest-farthest scheme, gives us, i.e.,

$$\text{Random}: \qquad \Pr(C_u^{\text{com}} \leq C_{\text{th}}) = (1 - a^2) \qquad (4.27)$$

$$\text{Nearest} - \text{Farthest}: \qquad \Pr(C_u^{\text{com}} \leq C_{\text{th}}) = (1 - a^N) \qquad (4.28)$$

where, $a = \frac{1}{R^2}\left(\frac{\gamma_{\text{th}}^{\text{com}}\sigma^2}{p_2 - \gamma_{\text{th}}^{\text{com}}(p_1+p_2)}\right)^{-\frac{2}{\alpha}}$. Now substituting (4.24) and (4.27) in (4.13) for random scheme, and (4.25) and (4.28) in (4.13) for nearest- farthest scheme, the OP for the near user can be given as follows:

$$\text{Random}: \qquad \mathcal{O}_1^{\text{RF}} = (1 - b)^2(1 - a^2) \qquad (4.29)$$

$$\text{Nearest} - \text{Farthest}: \qquad \mathcal{O}_1^{\text{RF}} = (1 - b)^N(1 - a^N) \qquad (4.30)$$

where $b = \frac{1}{R^2}\left(\frac{\gamma_{\text{th}}^{\text{pr}}\sigma^2}{(p_1 - \gamma_{\text{th}}^{\text{pr}}p_2)}\right)^{-\frac{2}{\alpha}}$.

4.4.2 Far User

Based on (4.7), the OP for private message of far user can be formulated as:

$$\Pr\left(\gamma_2^{\mathrm{pr}} \leq \gamma_{\mathrm{th}}^{\mathrm{pr}}\right) = \Pr\left(h_2 \leq \frac{\gamma_{\mathrm{th}}^{\mathrm{pr}}\sigma^2}{p_2 - \gamma_{\mathrm{th}}^{\mathrm{pr}}p_1}\right) \tag{4.31}$$

Now by substituting (4.3) in (4.31), I get:

$$\begin{aligned}\Pr\left(\gamma_2^{\mathrm{pr}} \leq \gamma_{\mathrm{th}}^{\mathrm{pr}}\right) &= \Pr\left(d_2 \geq \left(\frac{\gamma_{\mathrm{th}}^{\mathrm{pr}}\sigma^2}{p_2 - \gamma_{\mathrm{th}}^{\mathrm{pr}}p_1}\right)^{-\frac{1}{\alpha}}\right) \\ &= 1 - F_{d_2}\left[\left(\frac{\gamma_{\mathrm{th}}^{\mathrm{pr}}\sigma^2}{p_2 - \gamma_{\mathrm{th}}^{\mathrm{pr}}p_1}\right)^{-\frac{1}{\alpha}}\right]\end{aligned} \tag{4.32}$$

Now substituting (3.13) in (4.32) for random scheme, and (3.15) in (4.32) for nearest-farthest scheme, yield the OP of the private message of U_2, as given below:

$$\text{Random}: \qquad \Pr\left(\gamma_2^{\mathrm{pr}} \leq \gamma_{\mathrm{th}}^{\mathrm{pr}}\right) = 1 - \frac{1}{R^4}\left(\frac{\gamma_{\mathrm{th}}^{\mathrm{pr}}\sigma^2}{\gamma_{\mathrm{th}}^{\mathrm{pr}}p_1 - p_2}\right)^{-\frac{4}{\alpha}} \tag{4.33}$$

$$\text{Nearest} - \text{Farthest}: \qquad \Pr\left(\gamma_2^{\mathrm{pr}} \leq \gamma_{\mathrm{th}}^{\mathrm{pr}}\right) = 1 - \frac{1}{R^2}\left(\frac{\gamma_{\mathrm{th}}^{\mathrm{pr}}\sigma^2}{\gamma_{\mathrm{th}}^{\mathrm{pr}}p_1 - p_2}\right)^{-\frac{2N}{\alpha}} \tag{4.34}$$

The OP for common message for U_2 as given in (4.29) and (4.30) for random and nearest-farthest schemes, respectively. The OP for U_2 can then be calculated as:

$$\text{Random}: \qquad \mathcal{O}_2^{\mathrm{RF}} = (1-b')^2(1-a^2) \tag{4.35}$$

$$\text{Nearest} - \text{Farthest}: \qquad \mathcal{O}_2^{\mathrm{RF}} = (1-b')^N(1-a^N) \tag{4.36}$$

where, $b' = \frac{1}{R^2}\left(\frac{\gamma_{\mathrm{th}}^{\mathrm{pr}}\sigma^2}{\gamma_{\mathrm{th}}^{\mathrm{pr}}p_1 - p_2}\right)^{-\frac{2}{\alpha}}$.

4.5 Outage Analysis: RSMA-THz Network

4.5.1 Near User

Based on (4.6), $\Pr(\gamma_1^{\mathrm{pr}} \leq \gamma_{\mathrm{th}}^{\mathrm{pr}})$ can be equivalently rewritten as:

$$\Pr\left(\gamma_1^{\mathrm{pr}} \leq \gamma_{\mathrm{th}}^{\mathrm{pr}}\right) = \Pr\left(h_1 \leq \frac{\gamma_{\mathrm{th}}^{\mathrm{pr}} N_1^{\mathrm{pr}}}{\chi_1(p_1 - \gamma_{\mathrm{th}}^{\mathrm{pr}} p_2)}\right) \tag{4.37}$$

Substituting (4.2) and (4.8) in (4.37), I have the following:

$$\begin{aligned}\Pr\left(\gamma_1^{\mathrm{pr}} \leq \gamma_{\mathrm{th}}^{\mathrm{pr}}\right) &= \Pr\left(\chi_1 \leq \frac{\gamma_{\mathrm{th}}^{\mathrm{pr}} k_b T d_1^2}{\zeta e^{-k_a(f)d_1}\left(1 + p_1 - \gamma_{\mathrm{th}}^{\mathrm{pr}} p_2) - 1\right)}\right) \\ &= \int_0^R \frac{\gamma\left[m, \frac{1}{\Theta}\frac{\gamma_{\mathrm{th}}^{\mathrm{pr}} k_b T d_1^2}{\zeta e^{-k_a(f)d_1}\left(1+p_1-\gamma_{\mathrm{th}}^{\mathrm{pr}} p_2)-1\right)}\right]}{\Gamma(m)} f_{d_1}(d_1)\, dd_1, \end{aligned} \tag{4.38}$$

where $\gamma(\cdot)$ is the lower incomplete Gamma function, $\Gamma(\cdot)$ is the complete Gamma function, m is the fading severity parameter, Θ is the fading power. Since $k_b T$ is negligible compared to molecular noise, the OP for private message is written as:

$$\begin{aligned}\Pr\left(\gamma_1^{\mathrm{pr}} \leq \gamma_{\mathrm{th}}^{\mathrm{pr}}\right) &= \Pr\left(\frac{e^{-k(f)d_1}}{\frac{p_2}{p_1} + 1 - e^{-k(f)d_1}} \leq \gamma_{\mathrm{th}}^{\mathrm{pr}}\right) \\ &= \Pr\left(d_1 \geq \frac{1}{k(f)} \ln\left(\frac{1 + \gamma_{\mathrm{th}}^{\mathrm{pr}}}{(\frac{p_2}{p_1} + 1)\gamma_{\mathrm{th}}^{\mathrm{pr}}}\right)\right) \\ &= 1 - F_{d_1}\left(\frac{1}{k(f)} \ln\left[\frac{1 + \gamma_{\mathrm{th}}^{\mathrm{pr}}}{(\frac{p_2}{p_1} + 1)\gamma_{\mathrm{th}}^{\mathrm{pr}}}\right]\right). \end{aligned} \tag{4.39}$$

Now substituting (3.13) in (4.39) for random scheme, and (3.15) in (4.39) for nearest-farthest scheme, gives the OP of the private message of U_1 as shown below:

$$\text{Random}: \quad \Pr\left(\gamma_1^{\text{pr}} \leq \gamma_{\text{th}}^{\text{pr}}\right) = \left[1 - \left(\frac{1}{Rk(f)} \ln\left[\frac{1+\gamma_{\text{th}}^{\text{pr}}}{(\frac{p_2}{p_1}+1)\gamma_{\text{th}}^{\text{pr}}}\right]\right)^2\right]^2 \tag{4.40}$$

$$\text{Nearest} - \text{Farthest}: \quad \Pr\left(\gamma_1^{\text{pr}} \leq \gamma_{\text{th}}^{\text{pr}}\right) = \left[1 - \left(\frac{1}{Rk(f)} \ln\left[\frac{1+\gamma_{\text{th}}^{\text{pr}}}{(\frac{p_2}{p_1}+1)\gamma_{\text{th}}^{\text{pr}}}\right]\right)^2\right]^N. \tag{4.41}$$

By calling (4.19) and given that $\Pr(R_u^{\text{c}} \leq 2C_{\text{th}}) = \Pr\left(\gamma_u^c \leq \gamma_{\text{th}}^{\text{com}}\right), \quad \forall u = \{1, 2\}$, where, $\gamma_{\text{th}}^{\text{com}} = 2^{\frac{2C_{\text{th}}}{B}} - 1$, we can calculate the OP of common message in RSMA-THz as:

$$\begin{aligned}
&\Pr(C_u^{\text{com}} \leq C_{\text{th}}) = 1 - \Pr\left(\gamma_2^c \geq \gamma_{\text{th}}^{\text{com}}\right) \\
&= 1 - \Pr\left(h_1 \geq \frac{\gamma_{\text{th}}^{\text{com}}\sigma^2}{p_c - \gamma_{\text{th}}^{\text{com}}(p_1+p_2)}\right) \\
&= 1 - \Pr\left(d_2 \leq \left(\frac{1}{k(f)} \ln\left(\frac{p_c + \gamma_{\text{th}}^{\text{com}} p_c}{\gamma_{\text{th}}^{\text{com}}}\right)\right)\right) \\
&= 1 - F_{d_2}\left[\frac{1}{k(f)} \ln\left(\frac{p_c + \gamma_{\text{th}}^{\text{com}} p_c}{\gamma_{\text{th}}^{\text{com}}}\right)\right]
\end{aligned} \tag{4.42}$$

By substituting (3.13) in (4.42) for random scheme, and (3.15) in (4.42) for nearest-farthest scheme, gives us, i.e.,

$$\text{Random}: \qquad \Pr(C_u^{\text{com}} \leq C_{\text{th}}) = (1 - v^2) \tag{4.43}$$

$$\text{Nearest} - \text{Farthest}: \qquad \Pr(C_u^{\text{com}} \leq C_{\text{th}}) = (1 - v^N) \tag{4.44}$$

where, $v = \left[\frac{1}{Rk(f)} \ln\left(\frac{p_c+\gamma_{\text{th}}^{\text{com}} p_c}{\gamma_{\text{th}}^{\text{com}}}\right)\right]^2$. Now substituting (4.40) and (4.43) in (4.13) for random scheme, and (4.41) and (4.44) in (4.13) for nearest- farthest scheme, the OP for the near user can be given as follows: The outage of U_1 is given as:

$$\text{Random}: \qquad \mathcal{O}_1^{\text{THz}} = (1-w)^2(1-v^2) \tag{4.45}$$

$$\text{Nearest} - \text{Farthest}: \qquad \mathcal{O}_1^{\text{THz}} = (1-w)^N(1-v^N) \tag{4.46}$$

where, $w = \left[\frac{1}{Rk(f)} \ln\left(\frac{1+\gamma_{\text{th}}^{\text{pr}}}{(\frac{p_2}{p_1}+1)\gamma_{\text{th}}^{\text{pr}}}\right)\right]^2$.

4.5.2 Far User

Based on (4.7), $\text{P}(\gamma_2^{\text{pr}} \leq \gamma_{\text{th}}^{\text{pr}})$ can be formulated as follows:

$$\Pr\left(\gamma_2^{\text{pr}} \leq \gamma_{\text{th}}^{\text{pr}}\right) = \Pr\left(h_2 \leq \frac{\gamma_{\text{th}}^{\text{pr}} N_2^{\text{pr}}}{\chi_2(p_2 - \gamma_{\text{th}}^{\text{pr}} p_1)}\right) \tag{4.47}$$

Substituting (4.2) and (4.5) in (4.47), we get:

$$\begin{aligned}
\Pr\left(\gamma_2^{\text{pr}} \leq \gamma_{\text{th}}^{\text{pr}}\right) &= \Pr\left(\zeta d_2^{-2} e^{-k(f)d_2} \leq \frac{\gamma_{\text{th}}^{\text{pr}}\left(k_b T + (p_1+p_2)\zeta d_2^{-2}(1-e^{-k_a(f)d_2})\chi_2\right)}{\chi_2(p_2 - \gamma_{\text{th}}^{\text{pr}} p_1)}\right) \\
&= \Pr\left(\chi_2 \leq \frac{\gamma_{\text{th}}^{\text{pr}} k_b T d_2^2}{\zeta e^{-k_a(f)d_2}\left(1 + p_2 - \gamma_{\text{th}}^{\text{pr}} p_1\right) - 1)}\right) \\
&= \int_0^R \frac{\gamma\left[m, \frac{1}{\Theta}\frac{\gamma_{\text{th}}^{\text{pr}} k_b T d_2^2}{\zeta e^{-k_a(f)d_2}\left(1+p_2-\gamma_{\text{th}}^{\text{pr}} p_1\right)-1)}\right]}{\Gamma(m)} f_{d_2}(d_2)\, dd_2,
\end{aligned} \tag{4.48}$$

Since k_bT is negligible compared to molecular absorption noise, then, the OP of the private message of U_2 can be given as:

$$\begin{aligned}\Pr\left(\gamma_2^{\mathrm{pr}} \leq \gamma_{\mathrm{th}}^{\mathrm{pr}}\right) &= \Pr\left(\frac{e^{-k(f)d_2}}{\frac{p_1}{p_2}+1-e^{-k(f)d_2}} \leq \gamma_{\mathrm{th}}^{\mathrm{pr}}\right) \\ &= \Pr\left(d_2 \geq \frac{1}{k(f)} \ln\left[\frac{1+\gamma_{\mathrm{th}}^{\mathrm{pr}}}{(\frac{p_1}{p_2}+1)\gamma_{\mathrm{th}}^{\mathrm{pr}}}\right]\right) \\ &= 1 - F_{d_2}\left(\frac{1}{k(f)} \ln\left[\frac{1+\gamma_{\mathrm{th}}^{\mathrm{pr}}}{(\frac{p_1}{p_2}+1)\gamma_{\mathrm{th}}^{\mathrm{pr}}}\right]\right). \end{aligned} \tag{4.49}$$

Now substituting (3.14) in (4.49) for random scheme, and (3.16) in (4.49) for nearest-farthest scheme, gives the OP expressions for the private message as follows:

$$\text{Random}: \qquad \Pr\left(\gamma_2^{\mathrm{pr}} \leq \gamma_{\mathrm{th}}^{\mathrm{pr}}\right) = 1 - \left[\frac{1}{Rk(f)} \ln\left(\frac{1+\gamma_{\mathrm{th}}^{\mathrm{pr}}}{(\frac{p_1}{p_2}+1)\gamma_{\mathrm{th}}^{\mathrm{pr}}}\right)\right]^4 \tag{4.50}$$

$$\text{Nearest}-\text{Farthest}: \qquad \Pr\left(\gamma_2^{\mathrm{pr}} \leq \gamma_{\mathrm{th}}^{\mathrm{pr}}\right) = 1 - \left[\frac{1}{Rk(f)} \ln\left(\frac{1+\gamma_{\mathrm{th}}^{\mathrm{pr}}}{(\frac{p_1}{p_2}+1)\gamma_{\mathrm{th}}^{\mathrm{pr}}}\right)\right]^{2N} \tag{4.51}$$

The OP for common message for U_2 as given in (4.43) and (4.44) for random and nearest-farthest schemes, respectively. Thus, the OP for U_2 can then be calculated as:

$$\text{Random}: \qquad \mathcal{O}_2^{\mathrm{RF}} = (1-w')^2(1-v^2) \tag{4.52}$$

$$\text{Nearest}-\text{Farthest}: \qquad \mathcal{O}_2^{\mathrm{RF}} = (1-w')^N(1-v^N) \tag{4.53}$$

where, $w' = \left(\frac{1}{k(f)} \ln\left[\frac{1+\gamma_{\mathrm{th}}^{\mathrm{pr}}}{(\frac{p_1}{p_2}+1)\gamma_{\mathrm{th}}^{\mathrm{pr}}}\right]\right)^2$.

4.6 Numerical Results and Discussions

In this section, I compare the performance of U_1 and U_2 in RF-RSMA and THz-RSMA network. Unless stated otherwise, the parameters are listed herein. I consider 100 users are uniformly distributed in a circular disc. Note that our results are general for any arbitrary value of radius in the range 100 -120 m for RF-RSMA and in the range 25 -50 m for THz-RSMA network. The transmission bandwidths for RF-RSMA and THz-RSMA are 0.5 MHz and 0.5 GHz, respectively. The antenna gains G_t and G_r are set as 20 dB for THz AP. The AP transmit power is 1W, The power allocation coefficients are set as $p_1 = 0.2$, $p_2 = 0.25$ and $p_c = 1 - (p_1 + p_2)$. Nakagami-m fading parameter is set as 2 and $\Omega = 1$ with frequency 1 THz and $k(f) = 0.1$ m^{-1} considering water vapour molecules for THz-RSMA.

Figure 4.3 demonstrates the private , the common, and the total OP for U_1 and U_2 in RF-RSMA, as a function of cell-radius. Figure 4.3 validates (4.24), (4.33), (4.26), (4.29),and (4.35) for random scheme, as well, (4.25), (4.34), (4.28) (4.30),and (4.36) for Nearest-Farthest scheme through Monte-Carlo simulations. Clearly, the outage for common message is same for both users, whereas, the outage of private message for near user is low compared to the far user which is intuitive. Observe that Nearest-Farthest scheme perform better than random scheme for the near user, while it is the opposite for far user. Moreover, the OP increases with the increase the distance of the cell radius for both users in both schemes. Figure 4.4 demonstrates the OP of U_1 and U_2 as a function of the cell-radius in THz-RSMA and validates (4.40), (4.50), (4.43), (4.45) and (4.52) for random scheme (4.41), (4.51), (4.44), (4.46) and (4.53) for Nearest-Farthest scheme through Monte-Carlo simulations. It is shown that the values obtained through derived expressions (shown in circles), exactly match those

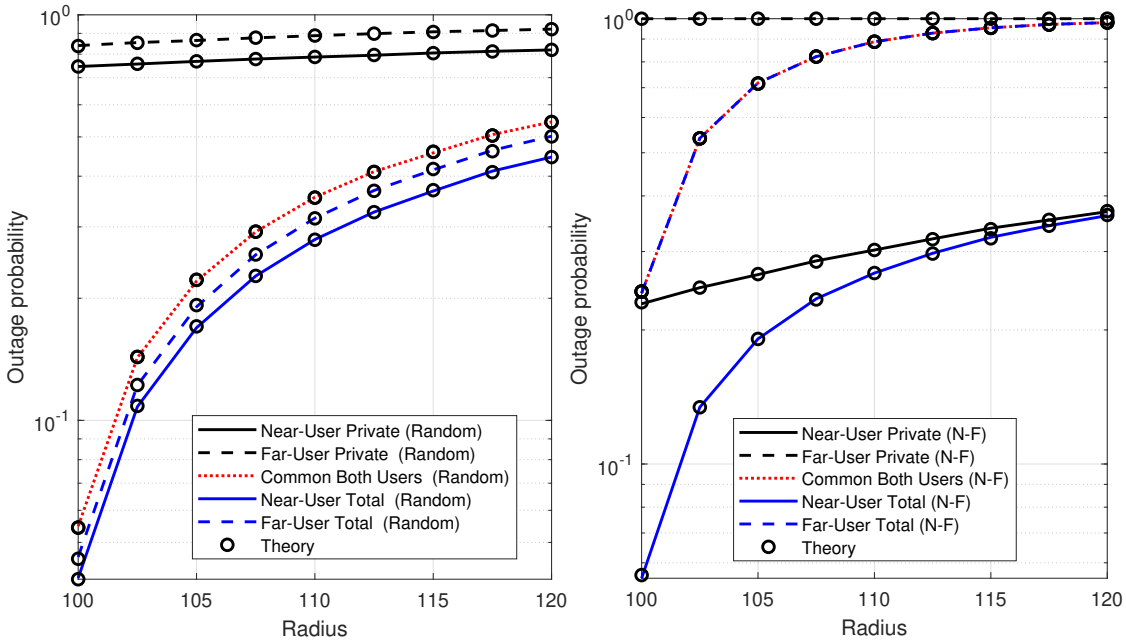

Figure 4.3: OP of near and far users as a function of the cell-radius, in RF spectrum where the power factors are given as p_1=0.20, p_2=0.25, and p_c=0.55.

obtained through simulations (shown by lines). It can be seen that the OP increases with the increase in the radius for both users. As expected, for near and far users with the increase in cell-radius, the OP increases.

Figure 4.5 demonstrates the OP of U_1 and U_2 as a function of the power allocation coefficient a_1 for NOMA and p_1 for RSMA and highlights the difference gain of RSMA, NOMA, and OMA. Note that to do that comparison, p_2 is considered to have a fix value ($p_2 = 0.25$), and $a_1 = p_1$. Observe that With the increase in a_1 and p_1, the OP increases for RSMA and NOMA due to the increased interference from U_1 observed at U_2. The gain of RSMA over NOMA and OMA improves more for low values of a_1 (p_1) for both near and far users for high values of a_1 (p_1) for both near and far users.

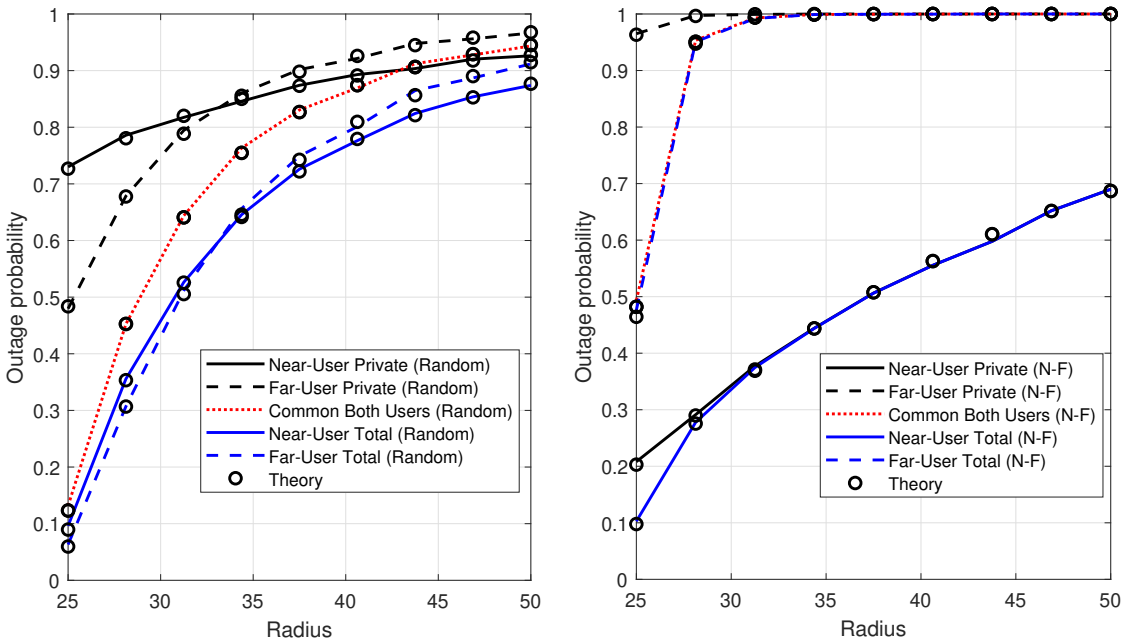

Figure 4.4: OP of near and far users as a function of the cell-radius in THz spectrum, where the power factors are $p_1 = 0.15, p_2 = 0.30, p_c = 0.55$.

4.7 Summary

I analyzed the performance of near and far users considering RF-RSMA and THz-RSMA networks. I have calculated the OP for each individual user considering the private and common messages as well as random and nearest-farthest user pairing schemes. The numerical results validate the accuracy of the derived expressions.

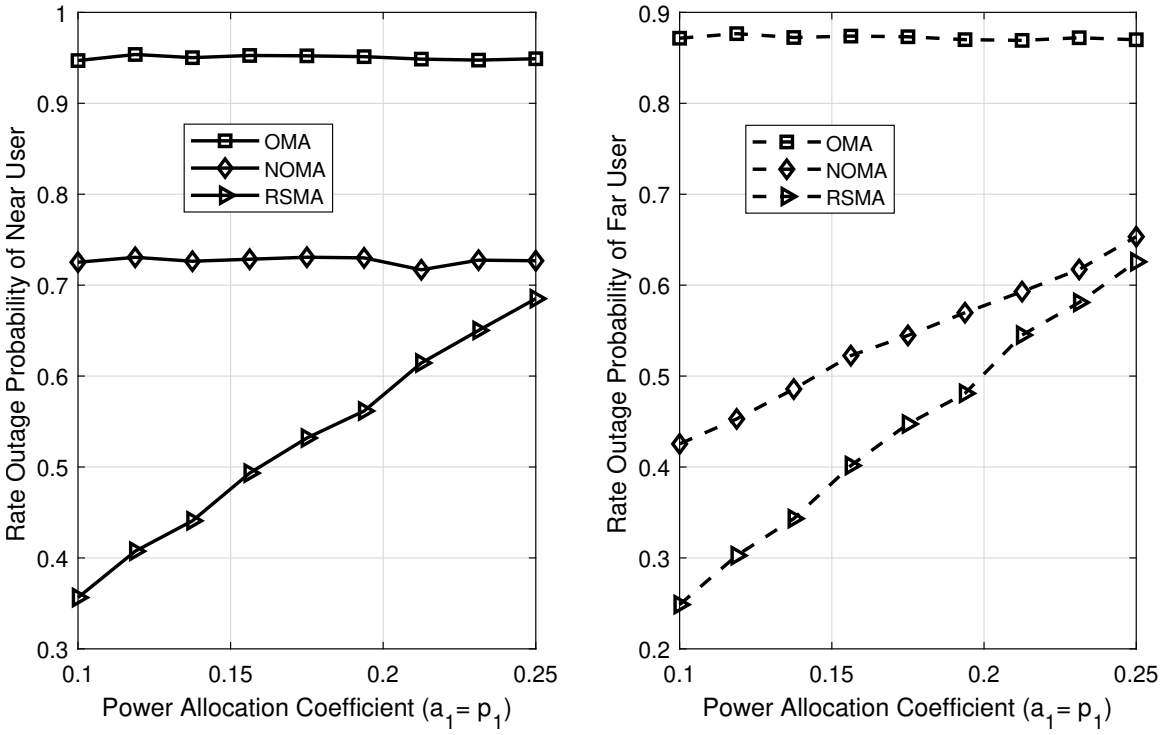

Figure 4.5: OP of near and far users as a function of power allocation spectrum in THz spectrum, for all multiple access schemes (OMA, NOMA, and RSMA), where radius $R = 60$, $p_2 = 0.25$, $ka = 0.03\, m^{-1}$ ($f_t = 0.8$ THz).

Chapter 5

Conclusions and Future Directions

5.1 Conclusion

This thesis presents a comprehensive framework for evaluating the performance of NOMA in single-carrier and multi-carrier THz networks in the downlink transmission. I focused on user performance in both THz-NOMA and THz-OMA schemes using single-carrier and multi-carrier setups. In a THz-NOMA network, I propose a unique user pairing technique that ensures NOMA over OMA performance increases for each user in the NOMA pair and compares it to random pairing and nearest-farthest approaches. Then, I identified the exact OP expressions in a single-carrier and multi-carrier THz-NOMA network considering Nakagami-m fading, capturing line-of-sight environment and molecular absorption noise. For the multi-carrier THz-NOMA network, I derived simplified single integral expressions from computing the OP. Furthermore, these expressions can be adapted to meet various user-pairing methods, and the resulting OP expressions are large enough to cover the whole THz spectrum. The numerical results further indicate the performance of the proposed user-pairing

scheme compared to benchmarks, validating the accuracy of my generated expressions.

5.2 Future Directions

The use of NOMA-THz in a next-generation (6G) environment is still in its early stages. To realise its impact on end users, a number of open issues and research problems must be solved. The outcomes explored in this thesis can be extended in the following ways:

5.2.1 Reducing NOMA Implementation Complexity

One of the significant problems of NOMA is its implementation complexity, which includes user pairing, signal decoding, and CSI acquisition, where the system's implementation complexity grows fast as the number of users increases. The unique features of NOMA allow for the development of several approaches that reduce the complexity of its implementation, perhaps making it more appropriate for practical use. As a result, for NOMA to be accepted by the industry, it must increase spectral efficiency and implementation feasibility.

5.2.2 Transmitter Design

One of the most challenging elements of adopting THz communication is transmitter design. Currently, electronics-based transmitters may operate in the 100–150 GHz region, demanding the creation of a higher-frequency transmitter. Designing power amplifiers at higher frequencies is also challenging. While waveform research in the THz band is now getting a lot of interest, researchers have yet to focus on deep

waveform schemes in the THz band. A potential issue in mobile applications is one of the most significant bandwidth elements of analog-to-digital converter design.

5.2.3 Imperfect CSI

Imperfect CSI is an open issue that should be addressed in order to decrease the impact of error. The researchers have already done much work using perfect CSI for resource allocation and multi-user detection. Due to feedback and channel estimate problems, perfect CSI is not available. It has been noticed that when a user's CSI is unknown, interference occurs. This occurred because, due to the limitations of imperfect CSI, signals received from other users could not be eliminated completely. Perfect joint precoders are required to eliminate interfering signals from the AP and more advanced channel estimation methods to get more precise channel information.

5.2.4 Non-line-of-sight (NLOS) propagation for THz networks

LOS communications may not always be possible due to the existence of obstacles. Representing the coefficients for EM wave reflection, scattering, and diffraction at THz frequencies is crucial to account for NLOS propagation. These coefficients are affected by the surface's material, shape, incident EM wave frequency, and angle. If LOS is not attainable, especially indoors, NLOS propagation serves as a backup. NLOS propagation can be created by carefully positioning installed dielectric mirrors to reflect the beam to the receiver. Due to the minimal reflection loss on dielectric mirrors, the resulting path loss is tolerable. For the THz spectrum, experimental measurements are required to verify the reflection, scattering, and diffraction coefficients for typical materials used for indoor and outdoor communications.

5.2.5 Multi-bands for 6G networks

THz spectrum will complement mm-wave and RF frequencies in 6G to transmit/receive data. Thanks to the variety of the spectrum which will cause a traded-off in terms of coverage area, capacity, user mobility, and latency. The main challenge will be in optimizing the deployment of APs, traffic load-aware network activation methods, opportunistic spectrum selection at the users' end, and multi-connectivity solutions.

5.2.6 Multi-Carrier RSMA-THz Network Performance:

The channel statistics for each sub-channel in THz spectrum suffers from distinct molecular absorption, as represented by the molecular absorption coefficient. As a result, the mathematical complexity of the Beer's-Lambert law-based channel propagation model on each sub-channel adds to the difficulty of outage analysis in a multi-carrier THz-RSMA network.

5.2.7 Novel User Pairing for THz-RSMA Network

It is also worth noting that assessing the performance of multi-carrier NOMA in RF networks is simple because all sub-channels have the same channel data. There is still no research that produces a low-complexity user pairing approach for the THz-RSMA network with a guaranteed gain over other multiple access techniques for each individual user and/or provides a complete framework for the outage analysis of users in a multi-carrier THz-RSMA network.

5.2.8 RSMA-THz Performance for Uplink Transmissions

Another open research topic is analyzing the performance of RSMA in a single-carrier and multi-carrier uplink transmissions in the THz networks.

5.2.9 Optimize User Clustering

In the downlink NOMA system, the user clustering and user scheduling [71] challenge is to optimize the total system throughput. In the future, it will be critical to investigate the best user clustering method with the least amount of computing complexity in various NOMA scenarios in THz networks.

5.2.10 NOMA Security

Since a single RB serves multiple devices in NOMA, which is handled via SC, security in NOMA is an essential problem that must be addressed in the next generation. Because it is subject to eavesdrop, the signal transfered through a wireless channel needs signifcant concern. The security of the physical layer is not fully exploited in NOMA; nonetheless, security remains an ongoing problem for the NOMA scheme.

5.2.11 Applying Machine Learning Technique:

Machine learning is a powerful tool for improving the performance of communication networks and improving the quality of experience for users, and it has the potential to revolutionize wireless resource allocation techniques by making them scalable [1]. ML will be one of the key techniques to be used for resource allocation (wireless spectrum and power allocations, user scheduling, and user association) in 6G networks. The ML methods might be distributed or centralised. In the first, users and APs submit

their local data to a central location, which results in communication costs, network resource consumption, privacy problems, etc. On the other hand, distributed ML (such as federated learning) is challenging because of the local computing and energy resource limitations, as well as the wireless communication dynamics that influence the global aggregation process. It is difficult to create a suitable global model for the non-identical facts. In addition, applying ML techniques to optimize the performance of the system and better user selection. Supervised learning or the k-mean algorithm is a powerful mechanism to determine each user's cluster.

5.2.12 THz Security

The THz band's inherent highly directed beam can enable secure communications, particularly for military applications. The directivity characteristic of the THz band, for instance, might limit the accessibility to support diverse users on a battlefield, such as infantry, armoured personnel carriers, and tanks. In contrast to lower band frequencies, which are spoofing, the THz band inherently implies safe communication based just on the network's structure, eliminating the need for tasking encryption techniques. However, to make use of this THz characteristic, beam alignment and beam tracking need to be investigated in the THz spectrum.

Bibliography

[1] S. B. Melhem, A. Kaushik, H. Tabassum, and U. T. Nguyen, "Machine learning for resource allocation in mobile broadband networks," *Communication Networks and Service Management in the Era of Artificial Intelligence and Machine Learning, Chapter.6, Wiley-IEEE Press*, pp. 123–146, 2021.

[2] H. Ibrahim, H. Tabassum, and U. T. Nguyen, "The meta distributions of the sir/snr and data rate in coexisting sub-6ghz and millimeter-wave cellular networks," *IEEE Open Journal of the Communications Society*, vol. 1, pp. 1213–1229, 2020.

[3] J. Sayehvand and H. Tabassum, "Interference and coverage analysis in coexisting RF and dense terahertz wireless networks," *IEEE Wireless Commun. Letters*, vol. 9, no. 10, pp. 1738–1742, 2020.

[4] H. Zarini, A. Khalili, H. Tabassum, and M. Rasti, "Joint transmission in qoe-driven backhaul-aware mc-noma cognitive radio network," in *GLOBECOM 2020-2020 IEEE Global Communications Conference*. IEEE, 2020, pp. 1–6.

[5] R. Hashemi, H. Beyranvand, M. R. Mili, A. Khalili, H. Tabassum, and D. W. K. Ng, "Energy efficiency maximization in the uplink delta-oma networks," *IEEE Transactions on Vehicular Technology*, vol. 70, no. 9, pp. 9566–9571, 2021.

[6] M. Rasti, S. K. Taskou, H. Tabassum, and E. Hossain, "Evolution toward 6g wireless networks: A resource management perspective," *arXiv preprint arXiv:2108.06527*, 2021.

[7] O. Semiari, W. Saad, M. Bennis, and M. Debbah, "Integrated millimeter wave and sub-6 GHz wireless networks: A roadmap for joint mobile broadband and ultra-reliable low-latency communications," *IEEE Wireless Commun.*, vol. 26, no. 2, pp. 109–115, 2019.

[8] H. Ibrahim, H. Tabassum, and U. T. Nguyen, "The meta distributions of the sir/snr and data rate in coexisting sub-6GHz and millimeter-wave cellular networks," *IEEE Open Journal of the Commun. Society*, vol. 1, pp. 1213–1229, 2020.

[9] M. Elkashlan, T. Q. Duong, and H. Chen, "Millimeter-wave commun. for 5G: fundamentals: Part i [guest editorial]," *IEEE Commun. Magazine*, vol. 52, no. 9, pp. 52–54, 2014.

[10] F. Khan, Z. Pi, and S. Rajagopal, "Millimeter-wave mobile broadband with large scale spatial processing for 5G mobile communication," in *2012 50th Annual Allerton Conference on Communication, Control, and Computing (Allerton)*, 2012, pp. 1517–1523.

[11] T. Rappaport, R. Heath, R. Daniels, and J. Murdock, *Millimeter wave wireless communications*. Prentice Hall, 2015, includes bibliographical references (pages 585-651) and index.

[12] I. A. Hemadeh, K. Satyanarayana, M. El-Hajjar, and L. Hanzo, "Millimeter-wave communications: Physical channel models, design considerations, antenna constructions, and link-budget," *IEEE Commun. Surveys Tutorials*, vol. 20, no. 2, pp. 870–913, 2018.

[13] H. Sarieddeen, N. Saeed, T. Y. Al-Naffouri, and M. Alouini, "Next generation Terahertz communications: A rendezvous of sensing, imaging, and localization," *IEEE Commun. Magazine*, vol. 58, no. 5, pp. 69–75, 2020.

[14] M. J. W. Rodwell, Y. Fang, J. Rode, J. Wu, B. Markman, S. T. Šuran Brunelli, J. Klamkin, and M. Urteaga, "100-340GHz systems: Transistors and applications," in *2018 IEEE Int.Electron Devices Meeting (IEDM)*, 2018, pp. 14.3.1–14.3.4.

[15] J. F. Harvey, M. B. Steer, and T. S. Rappaport, "Exploiting hiGH millimeter wave bands for military communications, applications, and design," *IEEE Access*, vol. 7, pp. 52 350–52 359, 2019.

[16] N. Hassan, M. T. Hossan, and H. Tabassum, "User association in coexisting rf and terahertz networks in 6g," in *2020 IEEE Canadian Conference on Electrical and Computer Engineering (CCECE)*. IEEE, 2020, pp. 1–5.

[17] L. Zhu, Z. Xiao, X. G. Xia, and D. Oliver Wu, "Millimeter-wave communications with non-orthogonal multiple access for b5G/6G," *IEEE Access*, vol. 7, pp. 116 123–116 132, 2019.

[18] K. Arora, J. SinGH, and Y. S. Randhawa, "A survey on channel coding techniques for 5G wireless networks," *Telecommunication Systems: Modelling,*

Analysis, Design and Management, vol. 73, no. 4, pp. 637–663, April 2020. [Online]. Available: https://ideas.repec.org/a/spr/telsys/v73y2020i4d10.1007_s11235-019-00630-3.html

[19] A. Goldsmith, *Spread Spectrum*. Cambridge University Press, 2005, p. 403–451.

[20] J. D. Vriendt, P. Laine, C. LeRouge, and X. Xu, "Mobile network evolution: a revolution on the move," *IEEE Commun. Mag.*, vol. 40, pp. 104–111, 2002.

[21] K. Raith and J. Uddenfeldt, "Capacity of digital cellular tdma systems," *IEEE Trans. on Vehicular Technology*, vol. 40, no. 2, pp. 323–332, 1991.

[22] O. Somekh and S. Shamai, "Shannon-theoretic approach to a gaussian cellular multiple-access channel with fading," *IEEE Trans. on Information Theory*, vol. 46, no. 4, pp. 1401–1425, 2000.

[23] J. De Vriendt, P. Laine, C. Lerouge, and X. Xu, "Mobile network evolution: a revolution on the move," *IEEE Communications Magazine*, vol. 40, no. 4, pp. 104–111, 2002.

[24] Y. OHWATARI, N. MIKI, T. ASAI, T. ABE, and H. TAOKA, "Performance of interference rejection combining receiver to suppress inter-cell interference in lte-advanced downlink," *IEICE Trans. on Commun.*, vol. E94.B, no. 12, pp. 3362–3369, 2011.

[25] H. Tabassum, M. S. Ali, E. Hossain, M. J. Hossain, and D. I. Kim, "Uplink vs. downlink NOMA in cellular networks: Challenges and research directions," in *2017 IEEE 85th Vehicular Technology Conference (VTC Spring)*, 2017, pp. 1–7.

[26] Y. Saito, Y. Kishiyama, A. Benjebbour, T. Nakamura, A. Li, and K. Higuchi, "Non-orthogonal multiple access (noma) for cellular future radio access," in *2013 IEEE 77th Vehicular Technology Conference (VTC Spring)*, 2013, pp. 1–5.

[27] S. Timotheou and I. Krikidis, "Fairness for non-orthogonal multiple access in 5g systems," *IEEE Signal Processing Letters*, vol. 22, no. 10, pp. 1647–1651, 2015.

[28] S. M. R. Islam, M. Zeng, O. A. Dobre, and K.-S. Kwak, "Non-orthogonal multiple access (noma): How it meets 5g and beyond," 2019.

[29] A. Bayesteh, E. Yi, H. Nikopour, and H. Baligh, "Blind detection of scma for uplink grant-free multiple-access," in *2014 11th International Symposium on Wireless Communications Systems (ISWCS)*, 2014, pp. 853–857.

[30] Y. Mao and B. Clerckx, *Multiple Access Techniques*. Cham: Springer Int.Publishing, 2021, pp. 63–100. [Online]. Available: https://doi.org/10.1007/978-3-030-58197-8_3

[31] Y. Mao, B. Clerckx, and V. O. Li, "Rate-splitting multiple access for downlink communication systems: bridging, generalizing, and outperforming sdma and NOMA," *EURASIP Journal on Wireless Communications and Networking*, vol. 2018, no. 1, May 2018. [Online]. Available: http://dx.doi.org/10.1186/s13638-018-1104-7

[32] B. Clerckx, H. Joudeh, C. Hao, M. Dai, and B. Rassouli, "Rate splitting for mimo wireless networks: a promising PHY-layer strategy for lte evolution," *IEEE Commun. Magazine*, vol. 54, no. 5, pp. 98–105, 2016.

[33] G. Zhou, Y. Mao, and B. Clerckx, "Rate-splitting multiple access for multi-antenna downlink communication systems: Spectral and energy efficiency trade-off," *IEEE Transactions on Wireless Communications*, pp. 1–1, 2021.

[34] Y. Mao, B. Clerckx, and V. O. Li, "Energy efficiency of rate-splitting multiple access, and performance benefits over sdma and noma," in *2018 15th International Symposium on Wireless Communication Systems (ISWCS)*, 2018, pp. 1–5.

[35] G. Zhou, Y. Mao, and B. Clerckx, "Rate-splitting multiple access for multi-antenna downlink communication systems: Spectral and energy efficiency trade-off," 2021.

[36] A. Rahmati, Y. Yapici, N. Rupasinghe, I. Guvenc, H. Dai, and A. Bhuyan, "Energy efficiency of rsma and noma in cellular-connected mmwave uav networks," in *2019 IEEE International Conference on Communications Workshops (ICC Workshops)*, 2019, pp. 1–6.

[37] M. Dai and B. Clerckx, "Multiuser millimeter wave beamforming strategies with quantized and statistical csit," *IEEE Transactions on Wireless Communications*, vol. 16, no. 11, pp. 7025–7038, 2017.

[38] C. Hao, Y. Wu, and B. Clerckx, "Rate analysis of two-receiver miso broadcast channel with finite rate feedback: A rate-splitting approach," *IEEE Transactions on Communications*, vol. 63, no. 9, pp. 3232–3246, 2015.

[39] I. F. Akyildiz, J. M. Jornet, and C. Han, "Terahertz band: Next frontier for wireless communications," *Physical Communication*, vol. 12, pp. 16–32,

2014. [Online]. Available: https://www.sciencedirect.com/science/article/pii/S1874490714000238

[40] S. Li, M. Derakhshani, S. Lambotharan, and L. Hanzo, "Outage probability analysis for the multi-carrier NOMA downlink relying on statistical csi," *IEEE Trans. on Commun.*, vol. 68, no. 6, pp. 3572–3587, 2020.

[41] C. E. Shannon, "A mathematical theory of communication," *The Bell System Technical Journal*, vol. 27, no. 3, pp. 379–423, 1948.

[42] H. A. David and H. N. Nagaraja, *Order statistics*. John Wiley & Sons, 2004.

[43] G. Grimmett and D. Stirzaker, *Probability and random processes*. Oxford university press, 2020.

[44] J. Gil-Pelaez, "Note on the inversion theorem," *Biometrika*, vol. 38, no. 3/4, pp. 481–482, 1951. [Online]. Available: http://www.jstor.org/stable/2332598

[45] B. Xia, J. Wang, K. Xiao, Y. Gao, Y. Yao, and S. Ma, "Outage performance analysis for the advanced sic receiver in wireless NOMA systems," *IEEE Trans. on Vehicular Technology*, vol. 67, no. 7, pp. 6711–6715, 2018.

[46] Z. Ding, Z. Yang, P. Fan, and H. V. Poor, "On the performance of non-orthogonal multiple access in 5G systems with randomly deployed users," *IEEE Signal Process. Lett.*, vol. 21, no. 12, pp. 1501–1505, 2014.

[47] H. Zhang, H. Zhang, W. Liu, K. Long, J. Dong, and V. C. M. Leung, "Energy efficient user clustering, hybrid precoding and power optimization in terahertz mimo-noma systems," *IEEE Journal on Selected Areas in Communications*, vol. 38, no. 9, pp. 2074–2085, 2020.

[48] S. R. Sabuj, A. M. S. Khan, and M. Hamamura, "Application of non-orthogonal multiple access for machine type communication in sub-Terahertz band," *Comput. Netw.*, vol. 182, p. 107508, 2020.

[49] O. Maraqa et al, "Energy-efficient coverage enhancement of indoor THz-MISO systems: An FD-NOMA approach," in *2021 IEEE 32nd Annu. Int. Symp. Pers., Indoor, Mobile Radio Commun (PIMRC)*, 2021, pp. 483–489.

[50] O. Ülgen, S. Erküçük, and T. Baykaş, "Non-orthogonal multiple access for terahertz communication networks," in *2020 11th IEEE Annual Ubiquitous Computing, Electronics Mobile Communication Conference (UEMCON)*, 2020, pp. 0737–0742.

[51] X. Zhang, C. Han, and X. Wang, "Joint beamforming-power-bandwidth allocation in terahertz noma networks," in *2019 16th Annual IEEE International Conference on Sensing, Communication, and Networking (SECON)*, 2019, pp. 1–9.

[52] Z. Yang, M. Chen, W. Saad, and M. Shikh-Bahaei, "Downlink sum-rate maximization for rate splitting multiple access (rsma)," in *ICC 2020 - 2020 IEEE International Conference on Communications (ICC)*, 2020, pp. 1–6.

[53] Z. Yang, M. Chen, W. Saad, W. Xu, and M. Shikh-Bahaei, "Sum-rate maximization of uplink rate splitting multiple access (rsma) communication," 2019.

[54] D. Yu, J. Kim, and S.-H. Park, "An efficient rate-splitting multiple access scheme for the downlink of c-ran systems," *IEEE Wireless Communications Letters*, vol. 8, no. 6, pp. 1555–1558, 2019.

[55] Z. Yang, M. Chen, W. Saad, and M. Shikh-Bahaei, "Optimization of rate allocation and power control for rate splitting multiple access (rsma)," *IEEE Transactions on Communications*, vol. 69, no. 9, pp. 5988–6002, 2021.

[56] L. Li, K. Chai, J. Li, and X. Li, "Resource allocation for multicarrier rate-splitting multiple access system," *IEEE Access*, vol. 8, pp. 174 222–174 232, 2020.

[57] Z. Yang, J. Shi, Z. Li, M. Chen, W. Xu, and M. Shikh-Bahaei, "Energy efficient rate splitting multiple access (rsma) with reconfigurable intelligent surface," in *2020 IEEE International Conference on Communications Workshops (ICC Workshops)*, 2020, pp. 1–6.

[58] L. Yin and B. Clerckx, "Rate-splitting multiple access for multibeam satellite communications," in *2020 IEEE International Conference on Communications Workshops (ICC Workshops)*, 2020, pp. 1–6.

[59] Y. Mao, B. Clerckx, and V. O. Li, "Rate-splitting multiple access for downlink communication systems: bridging, generalizing, and outperforming sdma and noma," *EURASIP journal on wireless communications and networking*, vol. 2018, no. 1, pp. 1–54, 2018.

[60] S. K. Singh, K. Agrawal, K. Singh, and C.-P. Li, "Outage probability and throughput analysis of uav-assisted rate-splitting multiple access," *IEEE Wireless Communications Letters*, vol. 10, no. 11, pp. 2528–2532, 2021.

[61] 3GPP, "Study on downlink multiuser superposition transmission (must) for lte (release 13)," in *TR36.859, Dec. 2015.*

[62] J. l. Lunine, "Atmospheric radiation. theoretical basis. r. m. goody and y. l. yung. second edition. oxford university press, new york, 1989. xvi, 519 pp., illus. 95," vol. 247, no. 4941, pp. 476–476, 1990. [Online]. Available: https://science.sciencemag.org/content/247/4941/476.1

[63] "The hitran2016 molecular spectroscopic database," *Journal of Quantitative Spectroscopy and Radiative Transfer*, vol. 203, pp. 3 – 69, 2017, hITRAN2016 Special Issue. [Online]. Available: http://www.sciencedirect.com/science/article/pii/S0022407317301073

[64] C. Han, A. O. Bicen, and I. F. Akyildiz, "Multi-ray channel modeling and wideband characterization for wireless communications in the terahertz band," *IEEE Trans. on Wireless Commun.*, vol. 14, no. 5, pp. 2402–2412, 2015.

[65] J. M. Jornet and I. F. Akyildiz, "Channel modeling and capacity analysis for electromagnetic wireless nanonetworks in the terahertz band," *IEEE Trans. on Wireless Commun.*, vol. 10, no. 10, pp. 3211–3221, 2011.

[66] A. Olutayo, J. Cheng, and J. F. Holzman, "A new statistical channel model for emerging wireless communication systems," *IEEE Open Journal of the Communications Society*, vol. 1, pp. 916–926, 2020.

[67] M. Di Renzo, "Stochastic geometry modeling and analysis of multi-tier millimeter wave cellular networks," *IEEE Transactions on Wireless Communications*, vol. 14, no. 9, pp. 5038–5057, 2015.

[68] J. G. Andrews, T. Bai, M. N. Kulkarni, A. Alkhateeb, A. K. Gupta, and R. W. Heath, "Modeling and analyzing millimeter wave cellular systems," *IEEE Transactions on Communications*, vol. 65, no. 1, pp. 403–430, 2017.

[69] N. Deng and M. Haenggi, "A fine-grained analysis of millimeter-wave device-to-device networks," *IEEE Transactions on Communications*, vol. 65, no. 11, pp. 4940–4954, 2017.

[70] A. Faisal et al., "Ultramassive MIMO systems at terahertz bands: Prospects and challenges," *IEEE Vehicular Tech. Magazine*, vol. 15, no. 4, pp. 33–42, 2020.

[71] H. Tabassum, E. Hossain, M. J. Hossain, and D. I. Kim, "On the spectral efficiency of multiuser scheduling in rf-powered uplink cellular networks," *IEEE transactions on wireless communications*, vol. 14, no. 7, pp. 3586–3600, 2015.

I Appendix A

I.1 Proof of Lemma 1

Starting from the condition $C_i^{(\text{noma})} > C_i^{(\text{oma})}$, $\forall i = \{1, 2\}$ and taking $\hat{T} = 1$ without loss of generality, I have:

$$\log_2\left(1 + \text{SINR}_i^{(\text{noma})}\right) > 0.5\log_2\left(1 + \text{SINR}_i^{(\text{oma})}\right), \forall i = \{1, 2\}. \tag{1}$$

Now, I substitute (3.8) and (3.12) in (1) for near user, and (3.9) and (3.12) in (1) for far user. After basic algebraic manipulations, I note that $d_1 < R_{\text{th1}}$ and $d_2 > R_{\text{th2}}$ are necessary conditions to guarantee the gains of NOMA over OMA for each individual user, where the value of R_{th1} and R_{th2} can be written as in (3.17) and (3.18), respectively.

I.2 Proof of Lemma 2

Since all users are uniformly distributed in a circular region of radius R, thus the PDF and CDF of a user from the BS r are given, respectively, as $f_r(r) = \frac{2r}{R^2}$ and $F_r(r) = \frac{r^2}{R^2}$. In the proposed scheme, the range of the near user is $d_1 \in [0, R_{\text{th1}}]$. Subsequently, d_1 follows the truncated distribution of r and its CDF can be calculated as follows:

$$F_{d_1}(d_1) = \frac{F_r(d_1) - F_r(0)}{F_r(R_{\text{th1}}) - F_r(0)} = \frac{\frac{{d_1}^2}{R^2} - \frac{(0)^2}{R^2}}{\frac{R_{\text{th1}}^2}{R^2} - \frac{(0)^2}{R^2}} = \frac{d_1^2}{R_{\text{th1}}^2},$$

Now, I can calculate the PDF by taking the derivative of the CDF as shown in **Lemma 2**. Similarly, the far user is located in the range $d_2 \in [R_{\text{th2}}, R]$ and the CDF

of d_2 is given as:

$$F_{d_2}(d_2) = \frac{F_r(d_2) - F_r(R_{\text{th2}})}{F_r(R) - F_r(R_{\text{th2}})} = \frac{d_2^2 - R_{\text{th2}}^2}{R^2 - R_{\text{th2}}^2},$$

Now, I can calculate the PDF of d_2 by taking the derivative of the CDF as shown in **Lemma 2**.

I.3 Proof of Lemma 3

From (3.28) and (3.29), I can write

$$W_{1,n} = 1 + \frac{B_1 \chi_{1,n} d_1^{-2} e^{-k(f_n)d_1}}{N_{1,n}^{(\text{noma})}} \tag{2}$$

$$W_{2,n} = 1 + \frac{B_2 \chi_{2,n} d_2^{-2} e^{-k(f_n)d_2}}{B_1 \chi_{2,n} d_2^{-2} e^{-k(f_n)d_2} + N_{2,n}^{(\text{noma})}} \tag{3}$$

For enhanced tractability, I ignore the thermal noise and obtain the following simplified results after algebraic manipulations for near and far users, respectively.

$$W_{1,n} = \frac{1}{1 - e^{-k(f_n)d_1}} \quad \text{or} \quad d_1 = \frac{1}{k(f_n)} \ln\left[\frac{W_{1,n}}{W_{1,n} - 1}\right],$$

$$W_{2,n} = \frac{1}{1 - a_2 e^{-k(f_n)d_2}} \quad \text{or} \quad d_2 = \frac{1}{k(f_n)} \ln\left[\frac{a_2 W_{2,n}}{W_{2,n} - 1}\right].$$

From (3.30) and using the fact that X_i is a constant conditional on d_i and the CDF of a constant is a unit-step function, I got to (3.35) as in **Lemma 3**.

II Appendix B

II.1 Proof of Corollary 1

To enhance the proposed scheme, we consider that the near user is the user with minimum distance, thus, $f_{d_1}(d_1)$ and $F_{d_1}(d_1)$ can be given as in (3.15). On the other hand, the far user is located beyond R_{th2}. So the range of the far user will be as $d_2 \in [R_{\text{th2}}, R]$, then in this case, $f_{d_2}(d_2)$ and $F_{d_2}(d_2)$ can be given as in (3.20).

II.2 Proof of Corollary 2

The near user will need to be located inside R_{th1}. However, each subcarrier will observe a different molecular absorption coefficient resulting in a different threshold distance R_{th1} at each subcarrier. Choosing the smallest threshold distance will not violate the threshold requirement of all other subcarriers, thus we consider $R_{\text{th1}}^{\min} = \min(R_{\text{th}_\text{n}}), \forall n \in \{1, 2, \cdots, N\}$ for near user. The range of d_1 becomes $d_1 \in [0, R_{\text{th1}}^{\min}]$, thus replacing R_{th1} with $R_{\text{th1}}^{\min}$ with in Lemma 2, we can obtain Corollary 2. Similarly, the far user will need to be located outside R_{th2}. Therefore, choosing the maximum threshold distance will not violate the threshold requirement of all other subcarriers, i.e., $R_{\text{th2}}^{\max} = \max(R_{\text{th}_\text{n}}), \forall n \in \{1, 2, \cdots, N\}$ for far user. The range of d_2 becomes $d_2 \in [0, R_{\text{th1}}^{\min}]$, thus replacing R_{th2} with $R_{\text{th2}}^{\max}$ in Lemma 2, we can obtain Corollary 2.